Journal of Rock Mechanics and Geotechnical Engineering 16 (2024) 3841–3863

Contents lists available at ScienceDirect

Journal of Rock Mechanics and Geotechnical Engineering

journal homepage: www.jrmge.cn

Review

Distributed fiber optic sensors for tunnel monitoring: A state-of-the-art review

Xuehui Zhang [a], Honghu Zhu [b], Xi Jiang [c], Wout Broere [a,*]

[a] Geo-Engineering Section, Department of Geoscience and Engineering, Delft University of Technology, Delft, 2628CN, the Netherlands
[b] School of Earth Sciences and Engineering, Nanjing University, Nanjing, 210023, China
[c] Department of Civil and Environmental Engineering, The Hong Kong Polytechnic University, Kowloon, Hong Kong, China

ARTICLE INFO

Article history:
Received 21 July 2023
Received in revised form
26 October 2023
Accepted 20 January 2024
Available online 27 March 2024

Keywords:
Distributed fiber optic sensor (DFOS)
Tunnel infrastructure
Distributed strain sensing
Point displacement monitoring
Field instrumentation

ABSTRACT

Distributed fiber optic sensors (DFOSs) possess the capability to measure strain and temperature variations over long distances, demonstrating outstanding potential for monitoring underground infrastructure. This study presents a state-of-the-art review of the DFOS applications for monitoring and assessing the deformation behavior of typical tunnel infrastructure, including bored tunnels, conventional tunnels, as well as immersed and cut-and-cover tunnels. DFOS systems based on Brillouin and Rayleigh scattering principles are both considered. When implementing DFOS monitoring, the fiber optic cable can be primarily installed along transverse and longitudinal directions to (1) measure distributed strains by continuously adhering the fiber to the structure's surface or embedding it in the lining, or (2) measure point displacements by spot-anchoring it on the lining surface. There are four critical aspects of DFOS monitoring, including proper selection of the sensing fiber, selection of the measuring principle for the specific application, design of an effective sensor layout, and establishment of robust field sensor instrumentation. These four issues are comprehensively discussed, and practical suggestions are provided for the implementation of DFOS in tunnel infrastructure monitoring.

1. Introduction

Underground infrastructure has emerged as an important component of the modern built environment. Various types of tunnels, such as metro and highway tunnels, logistic transport and services tunnels, as well as sewage tunnels, have long been constructed and operated. Especially in urban areas, these tunnel structures serve vital purposes, including expanding useable space, mitigating ground traffic congestion, and boosting urban resilience against climate change (Broere, 2016; Xu et al., 2019; Cui et al., 2021a). However, as the average service life of tunnels continues to increase, excessive structural deformation, cracking, leaking, and other structural deterioration indicators have frequently been observed during routine tunnel inspections (Yuan et al., 2012; Liu et al., 2018; Di Murro et al., 2019; Zhu et al., 2022). These signs of deterioration significantly undermine the long-term functionality and safety of tunnel infrastructure. As a result, effective monitoring of tunnel conditions and management of their structural health have become essential concerns for infrastructure asset managers and operators in recent years.

Structural health monitoring (SHM) generally refers to the continuous or periodic measurement and analysis of key structural and environmental parameters, for the purpose of signaling alerts of abnormal structural states or accidents at early stages (Housner et al., 1997). SHM has become a standard requirement for underground tunnel asset management, as a precise monitoring system in combination with reliable data interpretation techniques is a prerequisite for understanding a tunnel's structural behavior, facilitating condition assessment and predictive maintenance planning of tunnels (Xu et al., 2017; Buchmayer et al., 2021). In terms of the monitoring requirements, SHM should provide ample information on the actual status of the tunnel structure, thereby enabling geotechnical practitioners to make informed decisions on structural maintenance. The degree of "sufficiency of information" is typically determined by the spatial and temporal scope of data collection of the monitoring system.

* Corresponding author.
E-mail address: W.Broere@tudelft.nl (W. Broere).
Peer review under responsibility of Institute of Rock and Soil Mechanics, Chinese Academy of Sciences.

https://doi.org/10.1016/j.jrmge.2024.01.008

Modern deformation monitoring techniques for tunnels, whether under construction or in operation, can generally be categorized into three types: point-wise sensors, geodetic measurement, and three-dimensional (3D) laser scanning (Wang et al., 2023a). Since early times, point-wise sensors like resistance strain gauges, vibrating wire gauges (VWGs), and linear variable differential transformers (LVDTs) have been used to measure the local internal or exterior (surface) deformation of the tunnel lining (Radončić et al., 2015; Buchmayer et al., 2021). In geodetic measurements, points on the tunnel lining surface are usually marked with prism targets, and their displacements are monitored with a total station (Gue et al., 2015; Buchmayer et al., 2021). 3D laser scanning can capture the position changes of extremely dense (yet discrete) point clouds on the lining surface between two distinct data sampling intervals, further characterizing the overall deformation of tunnel linings (Roca-Pardinas et al., 2014). However, the aforementioned techniques for monitoring tunnel deformation have limitations in providing spatially and temporally adequate information on structural deformations. On one hand, both point-wise sensors and geodetic measurements only offer deformation information for discrete instrumented (or reference) points, exhibiting a substantial spatial limitation for monitoring long underground tunnels (Gómez et al., 2020; Wang et al., 2023a). On the other hand, while 3D laser scanning may collect the distributed deformation of the scanned surface, it requires expensive equipment and a sophisticated data-sampling operation, making it unfeasible to implement along the full length of the tunnel (Li et al., 2015) on a continuous basis. Addressing the spatial limitation is crucial for the optimization of conventional tunnel monitoring, and the distributed fiber optic sensor (DFOS) offers a competent solution to this challenge.

Distributed fiber optic sensor (DFOS) is a type of sensor that features superior capacities for distributed and long-distance sensing (López-Higuera et al., 2011; Motil et al., 2016). Typically, a complete DFOS system is composed of fiber optic cables (referred to as sensing cables, which can be up to one hundred kilometers in length) coupled with a terminal signal interrogator. The extended sensing distance makes it ideally suitable for instrumenting long underground tunnel infrastructures. When properly integrated into the structure being monitored, the system can capture densely distributed strain and temperature information (currently at sub-millimeter sampling intervals). Moreover, the sensing cable is relatively resistant to corrosion and other similar environmental impacts encountered in harsh underground environments. Therefore, the DFOS system can effectively address the spatial limitations inherent in current tunnel monitoring practices, providing a more desirable alternative for SHM of tunnels.

Recognizing these advantages, an increasing number of researchers have been exploring the application of DFOS in tunnel monitoring, both for tunnels under construction (De Battista et al., 2015; Seo et al., 2017; Monsberger et al., 2018) and those in operation (Soga, 2014; Wang et al., 2018; Zhu et al., 2022; Zhang and Broere, 2023a). These studies have collectively demonstrated the substantial potential of DFOS in practical monitoring applications. However, a dedicated review of DFOS applications for monitoring underground tunnel infrastructure is still lacking, and significant knowledge gaps persist. Specifically, these gaps revolve around the practical implementation of reliable and robust monitoring schemes adaptable to a variety of monitoring requirements.

This study presents a comprehensive review of prior advances in DFOS applications for deformation monitoring of underground tunnel infrastructure. Previous literature reviews on the use of DFOS in structural engineering (López-Higuera et al., 2011; Kechavarzi et al., 2015; Wijaya et al., 2021) and geotechnical engineering (Hong et al., 2017; Gong et al., 2019; Zheng et al., 2020; Ma et al., 2022) serve as valuable references for DFOS researchers. This review distinguishes itself by concentrating on the latest developments in DFOS applications for tunnel structures and focusing on the practical issues related to the selection, design, and implementation of a qualified field sensor setup. Firstly, the working principles of DFOS and the key technical metrics of the DFOS system will be outlined, including the preferred qualities of a sensing fiber and critical parameters of data-acquisition systems. Subsequently, an in-depth review of recent DFOS applications for monitoring tunnel infrastructure is presented, covering their use in bored tunnels, conventional tunnels constructed using the New Austrian Tunneling Method (NATM) or sprayed concrete lining (SCL), as well as immersed and cut-and-cover tunnels. Following this, the requirements of a robust sensor instrumentation scheme are analyzed and discussed, which serves as a useful design guideline for future DFOS applications.

2. Distributed fiber optic sensor (DFOS) system

A DFOS generally operates based on the optical backscattering phenomena of light propagation within an optical fiber, which includes (linear) Rayleigh scattering and (non-linear) Brillouin and Raman scattering (López-Higuera, 1998; Leung et al., 2015; Hartog, 2017). Notably, the Brillouin and Rayleigh backscattering phenomena are strain and temperature-dependent, which enables distributed strain and temperature sensing by analyzing the backscattered light signal (Motil et al., 2016). In contrast, Raman scattering is solely temperature-dependent, thereby enabling distributed temperature sensing. This has been successfully employed in various scenarios such as monitoring pipeline leaks (Wang et al., 2022, 2023c; Li et al., 2023) and tracking fire accidents in tunnels. While this study focuses on tunnel deformation monitoring via DFOS, primarily based on Brillouin and Rayleigh scattering principles within an optical fiber, it should be noted that Raman scattering is also an effective tool for hazard detection.

2.1. The working principle of DFOS based on Brillouin scattering

Due to interaction with the inner structure of the optical fiber, light propagating along an optical fiber will generate backscattered light, where the frequency of the backscattered light will shift (relative to that of the forward propagating light). In the case of the Brillouin scattering phenomenon, the resulting Brillouin frequency shift (BFS) is proportional to the strain and temperature applied on the optical fiber (López-Higuera et al., 2011; Motil et al., 2016). This relationship can be expressed as

$$\nu(T,\varepsilon) = C_\varepsilon(\varepsilon-\varepsilon_0) + C_T(T-T_0) + \nu_0(T_0,\varepsilon_0) \quad (1)$$

where $\nu(T,\varepsilon)$ is the BFS at temperature T and strain ε; C_ε is the strain sensitivity coefficient; C_T is the temperature sensitivity coefficient; and $\nu_0(T_0,\varepsilon_0)$ indicates the baseline BFS at the reference temperature T_0 and strain ε_0.

The optical sensing interrogator is used to determine the BFS by sampling the backscattered light and, depending on the traveling time of the light wave, determining the location where the backscattered light originated along the optical fiber. By measuring the BFS at various sampling points along the fiber, the spatially resolved strain or temperature information along the longitudinal direction can be obtained, as illustrated in Fig. 1. Given the hardware constraints of the interrogator, normally the BFS averaged over a

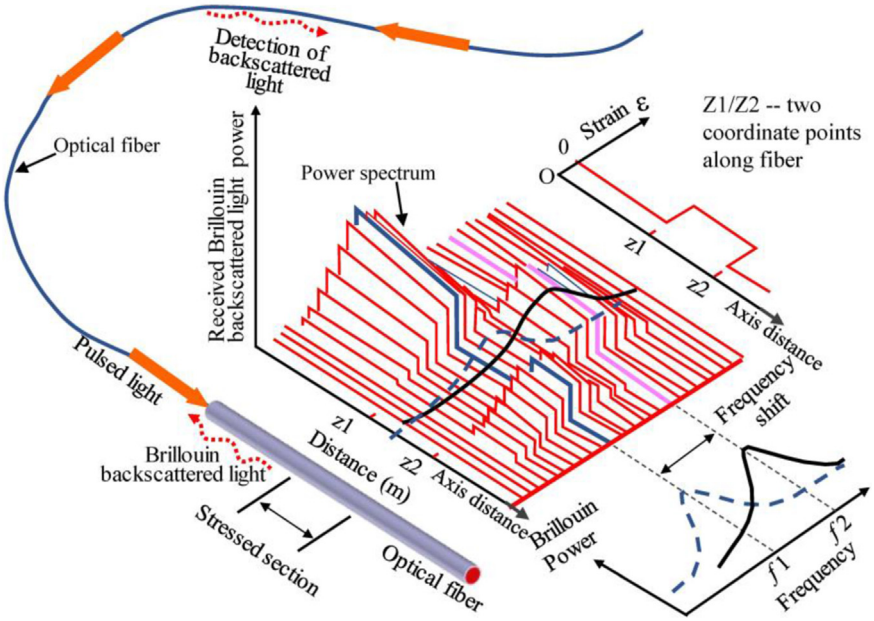

Fig. 1. Schematic of Brillouin scattering-based DFOS (*Z*1 and *Z*2 indicate two coordinate points along fiber, Zhu et al., 2022).

certain sampling length is obtained. This sampling length determines the spatial resolution of the strain and/or temperature measurement. The measuring accuracy and resolution of different types of commercially available interrogators will be further elaborated in Section 2.3.

2.2. The working principle of DFOS based on Rayleigh scattering

Rayleigh scattering in an optical fiber originates from the irregular microstructure of the fiber core, such as variations of the glass composition, resulting in fluctuations in the refractive index of the fiber core (Wuilpart, 2011; Tan et al., 2021). There are two widely used signal interpretation techniques for DFOS based on Rayleigh scattering, i.e. Optical Time Domain Reflectometry (OTDR) and Optical Frequency Domain Reflectometry (OFDR). However, OTDR has its limitations in reaching a relatively high spatial resolution (Leung et al., 2015). For distributed strain and temperature sensing, commercial interrogators mainly operate on OFDR, which measures the optical property variations between reference and the perturbed states.

In an OFDR interrogator, a light wave is beamed into the optical fiber to generate Rayleigh backscattering. The backscattered signal is detected (at the same end), and the amplitude of the backscattered signal is plotted against the wavelength of the light at each position along the fiber. The amplitude versus wavelength data is converted into an intensity versus frequency relation using a Fast Fourier Transform, followed by a cross-correlation of the reference and perturbed states, which determines the frequency shift for each location along the optical fiber (Kreger et al., 2006; Tan et al., 2021). This frequency shift is related to strain and temperature changes, as

$$\frac{\Delta\nu}{\nu} = \frac{\Delta\lambda}{\lambda} = K_\varepsilon(\varepsilon - \varepsilon_0) + K_T(T - T_0) \tag{2}$$

where λ and ν are the mean optical wavelength and frequency, and K_T and K_ε are the temperature and strain calibration constants, respectively.

2.3. Selection of optimal sensing fiber/cable

As an essential component of the DFOS system, the optical fiber serves as the direct sensing part as well as the signal transmission channel. Prior to selecting a specific type of sensing fiber, DFOS users should thoroughly understand the impact of optical fiber properties and the calibration work required.

In optical fiber manufacturing, the most basic product is the single-mode bare optical fiber, which normally is 0.25 mm in diameter (*D*-0.25 mm), as depicted in Fig. 2a, and is for instance manufactured by Corning (2021). In such fiber, the core and cladding form the pathway for light transmission, and these form the "sensing part" of the fiber, whilst the thin outer coating forms a protective layer. Another standard product is the 0.9 mm-diameter optical fiber (*D*-0.9 mm) made by adding a further protective outer buffer jacket to the bare *D*-0.25 mm fiber, as depicted in Fig. 2b. In addition, it is important to note that in distributed sensing applications, single-mode fibers (with a core diameter of 8–9 μm) are generally preferred over so-called multi-mode fibers (with a core diameter of about 50 μm), as the former tends to better maintain the optical signal intensity along the long fiber.

These *D*-0.9 mm fibers form the basis for both tight-buffered and loose-buffered fiber optic cables designed for indoor and outdoor use (as illustrated in Fig. 2c and d). These cables are shielded by an external jacket, sheath, or reinforcement parts (such as wires, strands, metal meshes, or metal tubes) for protection. The cost of the fiber optic cable often increases as the level of protection (or reinforcement) increases. The additional expense of the cables should be weighed against the potential risk of the application and the deployment environment, as will be discussed in Section 4. Whether a fiber optic cable is tightly or loosely buffered determines its application potential. In a tight-buffered cable, as shown in Fig. 2c, the inter-layer bonding permits inter-layer shear transfer that transfers external strain into the fiber core. On the other hand, a loose-buffered cable (as shown in Fig. 2d) can exhibit relative inter-layer slippage and as a result, the transmission of external strain to the fiber core is weak. Therefore, tight-buffered cables should be used for strain-sensing applications, whereas loose-

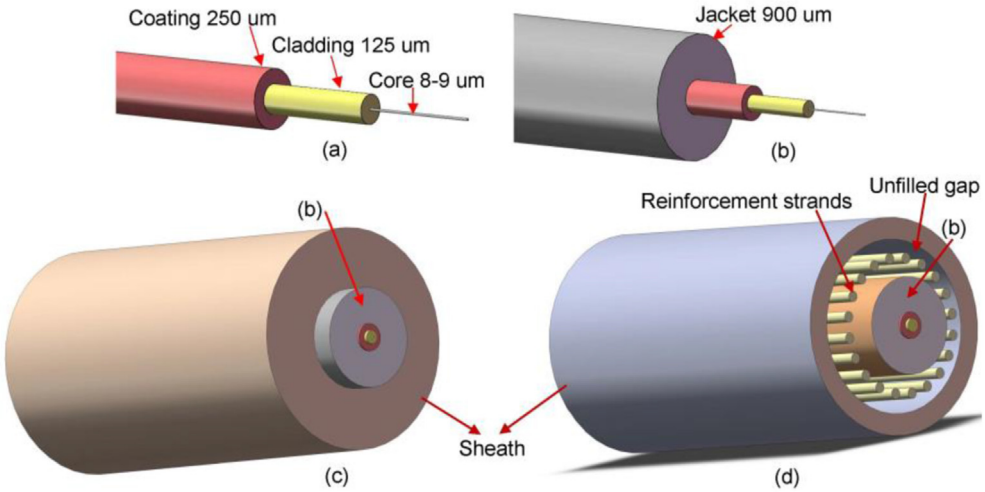

Fig. 2. Typical physical structures of optical fibers and cables: (a) *D*-0.25 mm bare fiber; (b) *D*-0.9 mm fiber; (c) Tight-buffered fiber optic cable; and (d) Loose-buffered fiber optic cable.

buffered cables, typically free of mechanical strain, are more suited for measuring temperatures.

A number of metrics exist for selecting prospective sensing fibers, such as (1) the maximum working strain; (2) the limit strain; (3) relaxation potential; (4) the strain and temperature sensitivity coefficient; and (5) the axial stiffness. To assure optimal sensing performance, the selected optical fiber and cable should be meticulously calibrated beforehand, and usually a characteristic curve is required to describe the relation of strain with the raw measurement quantity (e.g. Brillouin or Rayleigh frequency shift of backscattered signal), see Lienhart et al. (2014), Monsberger et al. (2018), and Zhang and Broere (2022).

A combined tension test is the most universal calibration method available, as described by Monsberger et al. (2018). In this test, a short fiber length is anchored at two sides and stepwise tensioned on a stretching platform (shown in Fig. 3), where one fiber anchorage translates along the sliding rail. A laser interferometer (or dial-gauges) measures the precise displacement (and hence the imposed fiber strain), while the force transducer measures the axial force in the fiber. The fiber ends are connected to the interrogator, and the (Brillouin or Rayleigh) frequency shift corresponding to each loading step can be obtained. From the imposed strain and tension force the frequency shift-strain (FS-ε) curve and force-strain (F-ε) curve can be obtained, from which the strain sensitivity coefficient and axial stiffness can be derived.

If the fiber optic cable has low axial stiffness and can be pre-strained manually, calibration can be conducted on a simple manual tension platform (as shown in Fig. 4) described in Zhang and Broere (2022). Short fiber lengths are anchored at two ends, where one anchorage can be translated, while the other end is fixed. In this setup, two dial gauges are used to measure the imposed displacement and correct for any in-plane tilting of the movable anchorage. The fiber ends are connected to an interrogator to measure the frequency shift, and multiple fibers can be evaluated simultaneously.

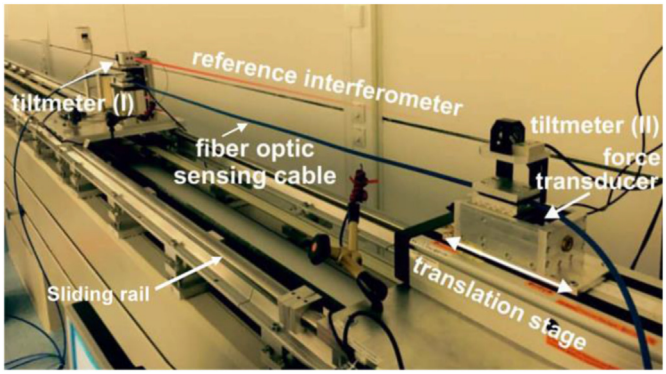

Fig. 3. Combined tension test platform for fiber optic cable calibration (Monsberger et al., 2018).

2.4. Overview of interrogator types for DFOS

The interrogator is a vital component of a DFOS system that determines the attainable measurement precision, provided that the sensing fibers are installed appropriately. The different interrogators described in the literature, as well as commercially available examples of these types, include.

(1) Interrogators operating on the principle of Brillouin Optic Time-Domain Reflectometry (BOTDR) or Brillouin Optic Time-Domain Analyzer (BOTDA), such as the NBX-6050/55 model from Neubrex Co., Ltd. (Neubrex, 2022), the DiTeST series from Omnisens (Smartec, 2022) and the DSTS from OZ Optics (OZ Optics, 2022).
(2) Interrogators operating on Brillouin Optic Frequency-Domain Reflectometry (BOFDR) or Brillouin Optic Frequency-Domain Analyzer (BOFDA), such as the fTB5020 model from Fibristerre (2022).
(3) Interrogators based on Brillouin Optic Correlation-Domain Analysis (BOCDA), which has no currently commercially available models. More details can be found in López-Higuera et al. (2011) and Motil et al. (2016).
(4) Interrogators operating on Optical Frequency Domain Reflectometry (OFDR), such as the OSI–S model (Megasense, 2022), the OBR4600 and ODiSI-610x model from Luna Innovations Inc. (Luna, 2022).

The main difference between these interrogator types, as their names indicate, lies in whether they operate in a time-domain or frequency-domain or follow another working principle, and whether (in the case of reflectometry) they use a single-ended optical fiber configuration and rely on the spontaneous

Fig. 4. Manual tension test platform.

backscattering of light within the fiber/cable, or (in the case of the analyzer types) rely on stimulated backscattering of light which requires a double-ended fiber loop where both ends are connected to the interrogator (Motil et al., 2016). An overview of the capabilities of interrogators documented in the literature is presented in Table 1.

The interrogator's performance requirements depend on the exact monitoring purposes, but several factors such as resolution and accuracy need to be carefully considered.

(1) Spatial resolution. Due to the way the light frequency is amplified in the interrogator, the measured frequency shifts, and therefore the derived strain or temperature for a given sampling location along the fiber optic cable is actually the weight-averaged value (centered on the sampling location) over the length of spatial resolution. This spatial resolution is the most critical system parameter, which determines the sensing precision. Currently, most commercial BOTDR and BODFR interrogators have a spatial resolution in the order of 1 m (between 0.5 m and 2 m), whilst that of the majority of BOTDA and BOFDA interrogators ranges from 0.1 m to 0.5 m. Moreover, an OFDR interrogator generally has a significantly better spatial resolution in the order of millimeters (Mega-sense, 2022; Luna, 2022).

(2) Maximum sensing distance (MSD). The maximum sensing distance is the maximum length of the optical fiber that can be used as a distributed sensor. Generally, the MSD of most Brillouin scattering-based interrogators is between 20 km and 100 km, while that of a commercial OFDR is much lower at around 100 m. It should be noted that for most interrogators, the spatial resolution capacity decreases with greater sensing distances. A trade-off between spatial resolution and MSD is needed when determining the suitable integrator type for a monitoring application.

Table 1
Overview of typical interrogator systems for distributed strain sensing.

Manufacturer	Interrogator Type	Working Principle	Key System Parameter Specifications					Application References
			Spatial resolution* (m)	Maximum sensing distance (km)	Sampling distance (m)	Strain range**and accuracy*	Temperature range** and accuracy*	
Smartec, Switzerland (Smartec, 2022)	DiTeST	BOTDA BOTDR	1–20 1.5–20	60 45	0.25	>5% 2×10^{-6}	−150 to 1000 °C 0.1 °C	Di Murro et al. (2019)
fibrisTerre, Germany (FibrisTerre, 2022)	fTB 5020/ 2505	BOFDA	0.2–2.5	80	0.05	−3% to 4% 2×10^{-6}	0.1 °C	Hou et al. (2021); Zhu et al. (2022);
		BOFDR	1.5	25		−0.2% to 4% 2×10^{-5}	1 °C	Zhang and Broere (2023a)
Neubrex, Japan (Neubrex, 2022)	NBX-6050A	BOTDA	0.05–1	25	0.01	−3% to 4% 7.5×10^{-6}	0.35 °C	Zhu et al. (2016); Zhang et al. (2020,2022b); Yang et al. (2023)
	NBX-6055A	BOTDA	0.05–1	25	0.01	−3% to 4% 7×10^{-6}	0.3 °C	Chai et al. (2021)
CECT, China (Ceyear, 2023)	AV6419	BOTDR	1	80	0.05	±1.5% 1×10^{-5}		Hou et al. (2017); Xue et al. (2019); Li et al. (2020)
OZ Optics, Canada (OZ Optics, 2022)	DSTS	BOTDA	0.1–50	160	0.05	−3% to 4% 2×10^{-6}	−270 to 2100 °C 0.1 °C	Wang et al. (2013)
		BOTDR	1–80	70		−0.2% to 1% 1.6×10^{-5}	−100 to 500 °C 0.8 °C	
Luna Innovations Inc., USA (Luna, 2022)	OBR4600/ ODiSi 610x	OFDR	0.00065 −0.01	0.01–0.2****	0.00065 −0.01	±1.5% 1×10^{-6}***	−40 to 200 °C 0.5 °C	Guo et al. (2023); Zhang et al. (2022a); Lu et al. (2023); Gómez et al. (2020)
Mega-sense Inc., China (Mega-sense, 2022)	OSI−S/OSI −C	OFDR	0.001–0.01	0.05–0.1****	0.001–0.01	±1.2% 1×10^{-6}***	−200 to 1200 °C 0.1 °C	Mo et al. (2022); Gao et al. (2023)

Note: * Varies with sensing distance; ** Strain/temperature range is typically fiber dependent; *** Dynamic sampling is possible; **** Extendable.

(3) Strain and temperature accuracy. The attainable accuracy of strain and temperature measurements for most interrogators lies below 20 micro-strain for strain and below 0.5 °C for temperature, which is more than adequate for common civil engineering monitoring tasks. In practice, the range of measurable strain and temperature for a DFOS system is determined more by the optical fiber used than the interrogator itself and depends primarily on aspects such as the cladding and protection offered by the buffering layers or any reinforcement of the cable itself.

(4) Sampling interval or sampling distance. The sampling interval indicates the distance between two data points based on the time gap between two consecutive light samples captured by the interrogator. A smaller sampling interval results in denser sampling points along the optical fiber and, therefore, richer sensing information. The smallest sampling interval achievable for most Brillouin scattering-based interrogators lies in the order of 10 cm, whereas that of an OFDR is in the order of millimeters.

(5) Other interrogator properties. Other aspects where a specific interrogator type can be preferred for a specific application are aspects like the availability of channel extensions allowing multiple sensing cables to be simultaneously attached to the interrogator, or the integration of a Raman scattering interrogator in a Brillouin interrogator which allows dedicated temperature measurements and corrections with a single device, as just a few examples. In general, the availability of such additional functions corresponds to a higher cost of the interrogator.

3. DFOS for monitoring tunnel infrastructure

Using a broad classification of the various applications in tunnel structural behavior monitoring, DFOS has been utilized either for (1) distributed strain sensing, where the fiber optic (FO) cable is continuously bonded on the structure's surface or embedded into the structure (see Fig. 5); and (2) relative point displacement monitoring (when functioning as an extensometer), where the cable is only fixed to the structure surface at discrete points, typically with an initially imposed prestrain on the (unbonded) interval fiber length between two fixed points (also referred to as the gauge length), as depicted in Fig. 5.

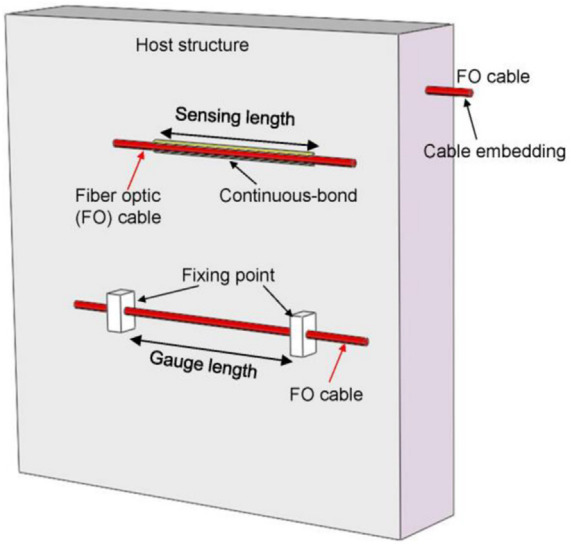

Fig. 5. Fiber optic (FO) cable instrumentation for distributed strain and point displacement sensing.

The distributed strain profile sensed by the embedded cable is the basis for interpreting the mechanical status (i.e. flexural deformation, axial deformation, evolution of cracks) of the tunnel lining under complex loading conditions during both construction and service periods. The fiber/cable used as extensometers can directly monitor locally concentrated deformations, typically at joint openings, and can be further assembled into a long extensometer chain for monitoring overall tunnel structural deformations.

The subsequent review focuses on DFOS applications in four types of tunnel structures that predominate in the available literature on this topic: bored tunnels, immersed tunnels, conventional tunnels constructed with the New Austrian Tunneling Method or Sprayed Concrete Lining method (henceforth for convenience referred to as NATM tunnels) and cut-and-cover tunnels. The literature used in this review consists of publications indexed in Scopus related to DFOS monitoring in tunnels and published since 2000. A search using the keywords ("tunnel" and "distributed optical fiber" or "distributed fiber optics") yields 105 publications (including journal articles and conference papers), which form the basis for this in-depth review. Notably, over 63% of these papers were published during the past five years (since 2018), and this is an indication of the rapid rise of DFOS applications in tunnel monitoring and its perceived competence.

3.1. Monitoring of bored tunnels

A bored tunnel is generally constructed with a tunnel boring machine (TBM), with prefabricated segments assembled on site to form the permanent tunnel lining. This results in a lining with radial joints between segments in a ring (see Figs. 6 and 7) and circumferential joints between adjoining rings (as shown in Fig. 8). These joints typically exhibit a lower flexural stiffness than the segment body itself, and thus, more significant deformation tends to concentrate on the joints when the tunnel is subject to flexural deformation transversely and longitudinally. In the structural health monitoring of a bored tunnel, the transverse and longitudinal deformation behaviors are critical aspects of monitoring work for assessing its structural states.

Transversely, the segmented lining subjected to surrounding ground loads exhibits a more significant flexural deformation mode, while the axial force on the cross-section also triggers compression or tension in the circumferential direction. This combined deformation can be interpreted by monitoring the distributed strain profile along the transverse cross-section, which is usually accomplished by embedding two parallel cables in the circumferential direction, on the inner and outer sides, of tunnel linings, as shown in Fig. 6a (Seo et al., 2017; Sui et al., 2022; Li et al., 2022). However, this embedding of fiber optic cable is only practical at the initial construction stage, while for existing tunnels distributed strain sensing is often limited to a continuously bonded cable on the inner surface (Gue et al., 2015; Gómez et al., 2020), as illustrated in Fig. 6b. In this way, the denser measurement grid achievable with DFOS enables engineers to better understand the stress and strain that develop on the lining compared to discrete pointwise measurements provided by conventional monitoring techniques.

In addition, a fiber optic cable can be fixed at several discrete points along the circumferential direction of a transverse section to build a chain of extensometers, see Fig. 6c. Such a sensing setup can help qualitatively monitor the transverse deformation behavior (oblique and vertical ovalization deformation), by analyzing the strain variations (between adjacent fixing points) measured by the

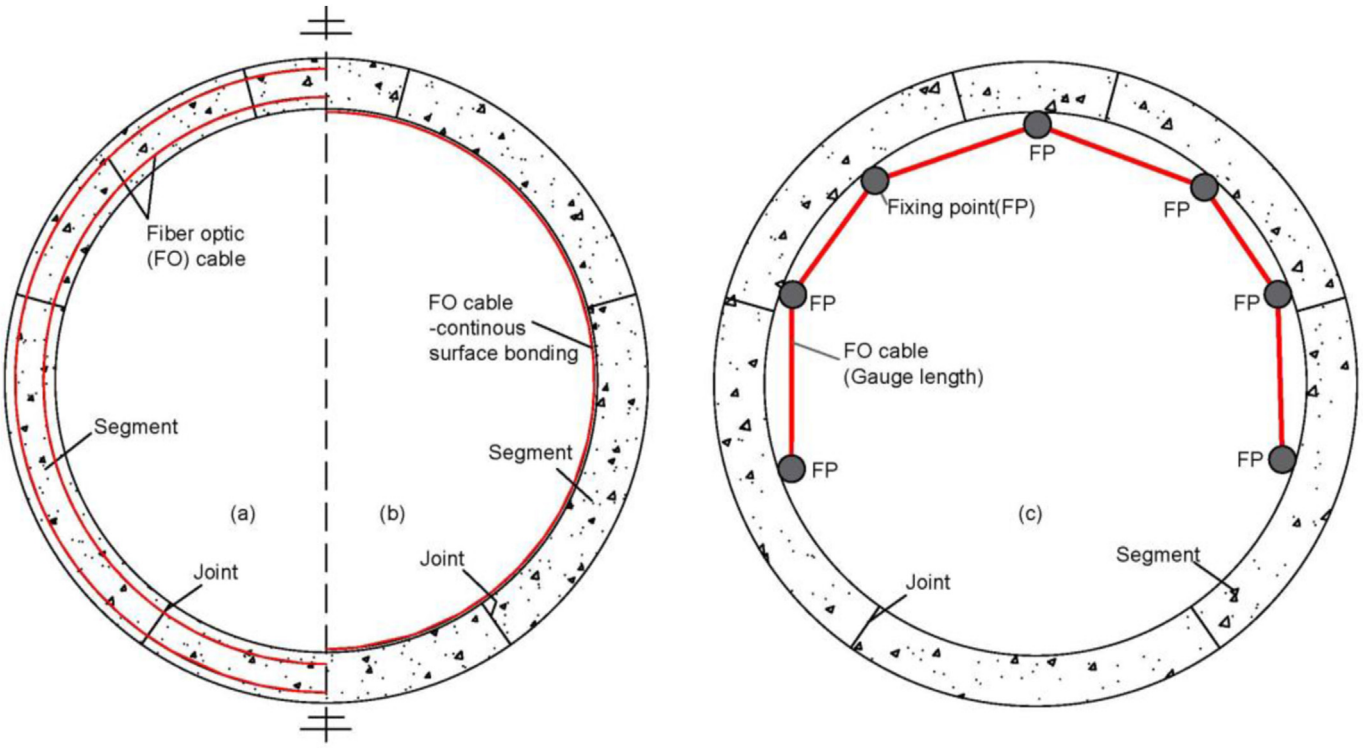

Fig. 6. DFOS for transverse behavior monitoring of bored tunnel: (a) embedded into the lining; (b) continuous bonding on intrados surface; (c) point-fixing on intrados surface for extensometers use.

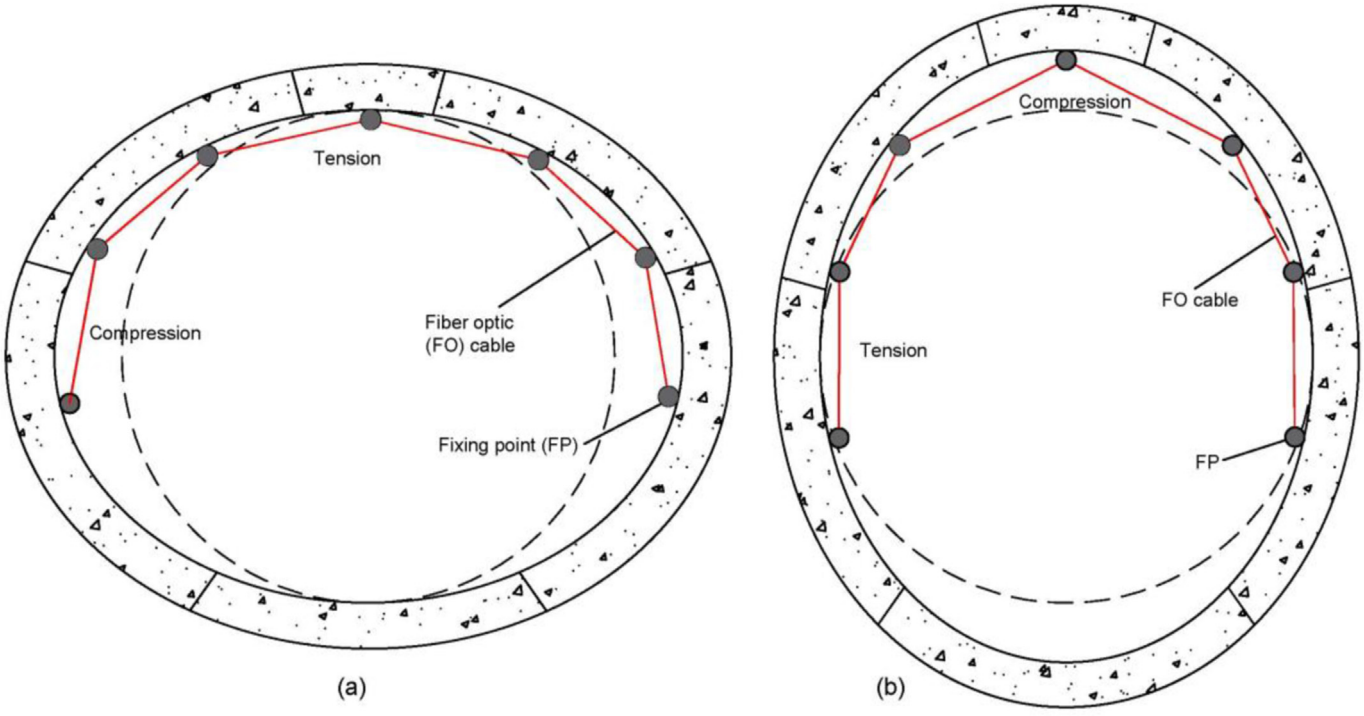

Fig. 7. Tunnel transverse distortion mode monitoring with DFOS: (a) oblique ovalization mode; and (b) vertical ovalization mode.

consecutively installed extensometers (as demonstrated in Fig. 7), see Gue et al. (2015), Acikgoz et al. (2017) and Zhu et al. (2022) for examples. Moreover, sometimes only the radial and circumferential joint deformations (the opening and closure at the joint) are of interest to assess the structural integrity and the risk of leakages, and in these cases, the fiber optic cable extensometer can be

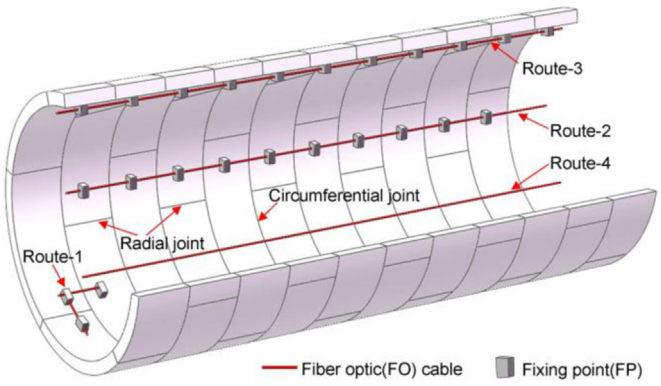

Fig. 8. Fiber optic extensometers for monitoring longitudinal deformation behavior of bored tunnels.

installed to span only the joint gap (see Route-1 in Fig. 8), as employed in Cheung et al. (2010), Wang et al. (2013) and Mo et al. (2022).

Longitudinally, a bored tunnel behaves more like a beam buried into the ground and it tends to exhibit flexural deformation when subjected to surrounding ground impacts such as differential settlements or movements induced by close-proximity construction activities. In general, it is difficult to capture the flexural behavior of a particularly long tunnel along its longitudinal axis. However, under bending deformation, the circumferential joint (the joint between two consecutive tunnel rings) expands or contracts depending on its location with respect to the hogging and sagging zones. This resultant joint deformation can be potentially detected by fiber optic extensometers mounted across the joint gap. Therefore, the opening deformation of circumferential joints, as sensed by the fiber optic extensometers at sidewalls (as Route-2 in Fig. 8), helps to understand the longitudinal bending behavior of the tunnel on the horizontal plane (Zhu et al., 2022), while a similar instrumentation scheme on the tunnel crown (as Route-3 in Fig. 8) helps to understand the bending deformation on the vertical plane (Gue et al., 2015). Furthermore, an additional cable route on the lower section of the tunnel, whether by continuously bonding (Li et al., 2021) (as Route-4 in Fig. 8) or point-fixing, helps provide more information on the tunnel behavior in the vertical plane. However, note that placing the cable at the tunnel invert is typically limited to tunnels under construction since the lower section is normally backfilled and paved.

(1) Distributed strain sensing

Shen et al. (2013) proposed a method to measure the convergence of shield tunnels based on distributed optical fiber strain sensing on the intrados surface, and its effectivity was investigated via a scaled laboratory experiment. Gue et al. (2015) installed a single-mode *D*-0.9 mm fiber by continuously gluing it along the circumferential direction on the inner lining surface of a bored tunnel with cast iron segments, to measure the distributed strain when a new tunnel was built beneath it. A BOTDR interrogator (spatial resolution of 1 m, strain accuracy of 3×10^{-6}) was used to collect the strain data, and measurement results show a maximum cumulative strain in both tension and compression in the order of 0.055%. This study demonstrates that when appropriately bonded, optical fibers can work effectively to obtain the distributed strain information along a tunnel lining.

In the study of Seo et al. (2017), a fiber optic cable was embedded into the concrete segment of a bored tunnel to evaluate the development of circumferential and longitudinal strain during and after the tunnel construction (as shown in Fig. 6a). A strongly reinforced cable (a Fujikura four-core fiber) was used for strain sensing, whilst an additional loose-buffer cable was used for temperature compensation. The strain difference on intrados and extrados of the lining is used to estimate the bending moment on the tunnel lining. In another study by Sui et al. (2022), the fiber optic cable is installed in a similar way to monitor the cross-section behavior of a newly-built large-diameter bored tunnel (11.2 m internal diameter), using a BOTDR with a spatial resolution of 1 m for data-acquisition. In the field monitoring campaigns of Li et al. (2022) and Hong et al. (2022), the fiber optic cable was located near the extrados of the lining by integrating it into the rebar cage prior to concrete casting, and this allowed for measuring the distributed strain development in the segmented lining.

Gómez et al. (2020) implemented DFOS to monitor the deformation of an in-service bored metro tunnel during the construction of a residential building above the tunnel. By continuously bonding to the inner lining surface, the optical fiber (with a sensing length of 50 m) instrumented a part of the circumferential perimeter of the tunnel at one transverse section (as shown in Fig. 6b) and a short portion of 8.7 m on the wall along the longitudinal tunnel axis. The strain was acquired through an OFDR interrogator type ODiSI-A manufactured by Luna Innovations Inc. In this case study, the interrogator had a set spatial resolution of 10 mm, and a maximum strain variation of about 1.7×10^{-4} was measured on the lining. The DFOS exhibited good performance in strain monitoring along the affected sections of tunnel lining. Li et al. (2021) glued the fiber optic cable continuously on the lower sidewall of a shield tunnel in the longitudinal direction, and the strain information was used to infer the tunnel's uneven settlement behavior.

Jiao and Zhou (2021) developed an optical-electrical co-sensing tape (OECST) by embedding a distributed optical fiber sensor (DOFS) and Fabry-Perot interferometer sensors (CCFPI) into an elastic polyurethane tape. The sensing performance of this tape was verified through a small-scale segment joint load test, with the tape continuously bonded on the segment surface. A BOTDA with a spatial resolution of 15 cm was adopted for strain sensing. Yang et al. (2023) proposed to identify the defects of shield tunnels based on circumferential strain sensing by DFOSs continuously bonded on the intrados. The effectivity of this approach is verified by a small-scale laboratory test, with a *D*-0.9 mm fiber for strain sensing and a BOTDA device of 10 cm spatial resolution.

Furthermore, Liu et al. (2020), Huang et al. (2021), and Wang et al. (2023a) applied fiber optic cables to monitor the performance of a water conveyance tunnel under internal pressure, which is constructed as a bored tunnel with an external diameter of 6 m and an average depth ranging from 40 m to 60 m underground. The tunnel is reinforced by a three-layer composite lining (the outer concrete segment lining, the internal steel tube, and the filling concrete in between) designed to enhance structural strength and prevent leakage. The fiber optic cable was placed circumferentially to continuously bond on the internal surface of the segment lining, the external circumference of the steel tube, and embedded into the filling concrete. A BOFDA interrogator was employed to collect strain data. In the subsequent internal pressure load test, the DFOS effectively detected the deformation and failure modes within the composite lining. Based on the monitoring results, an effective stiffness coefficient is proposed by Wang et al. (2023a) for describing the structural bearing performance.

In addition to field monitoring applications, DOFS have been used more and more in laboratory segment or joint load tests, due to the dense grid of strain sensing points it can provide. Monsberger et al. (2018) conducted laboratory bending tests on a single concrete segment instrumented with an embedded fiber optic cable.

The sensing fiber is aligned at the inner and outer sides of the cross-section and a high-resolution OFDR (type OBR4600 by Luna, with a spatial resolution of 10 mm) is used to collect the data. The results indicate the fiber optic cable can precisely measure the segment strain behavior as well as detect crack development inside the concrete during the loading process.

In the laboratory experiments of Zhang et al. (2022a) and Guo et al. (2023), DOFS was used to instrument scaled concrete segments and bolts in a joint performance test, where the fiber was continuously bonded on the bolt surface and the concrete surface, as well as embedded into the concrete by attaching it to the rebar. The strain data was sampled via an OFDR (type OBR4600), and the DOFS monitored the strain evolution throughout the loading test. Lu et al. (2023) used an optical fiber sensor to measure lining strain in a small-scale model test, where the sensing fiber is continuously glued both longitudinally and circumferentially along the external lining surface at a single transverse section, and an OFDR interrogator is used for strain sensing. The above studies demonstrate that DOFS, especially when combined with high-resolution OFDR interrogators, outperforms conventional point strain sensors in laboratory experiments.

(2) Extensometer use for point displacement monitoring

Cheung et al. (2010) implemented a *D*-0.9 mm optical fiber as extensometers across the radial joints of a bored tunnel for measuring joint opening and closure. The fiber was secured by separate pulleys nailed to the tunnel linings. A BOTDR with a 1 m spatial resolution recorded the strain variations and the joint openings were subsequently evaluated. Similar studies have been conducted by Wang et al. (2013), Mo et al. (2022), and Zhang et al. (2022b) to further investigate the performance and reliability of DOFS for complex joint deformation monitoring.

In another study, Mohamad et al. (2012) employed fiber optic cables to instrument a transverse cross-section of a bored tunnel (with an outer diameter of 6.35 m), to monitor its transverse distortion (ovalization) when a second bored tunnel was being constructed nearby. The cables were installed using a "hook and pulley" method, which involved inserting multiple hooks into the concrete lining with wall plugs and slotting a pulley onto each hook. The *D*-0.9 mm single-mode sensing cables were prestrained to 0.15% before being spot-glued to every pulley. A BOTDR type AQ8603 (Mohamad et al., 2010) recorded the highest compressive strain of 0.067% and the greatest tensile strain of 0.035%. Field monitoring confirmed that the DFOS, installed in this way, can distinguish the distortion mode of the tunnel's transverse cross-section.

Wang et al. (2018) and Zhu et al. (2022) instrumented a curved bored tunnel with a DFOS system to investigate its distortion and longitudinal behaviors during the excavation of a foundation pit in a dense urban area in China. Within a cross-section, a *D*-2 mm sensing cable (Nanzee Sensing, 2022) was fixed at discrete points (a gauge length of about 1 m) on the tunnel lining with specially designed block clamps made of stainless steel. The cable was prestrained to about 0.5% during field installation and used as extensometers across the circumferential joints at sidewalls. A BOFDA interrogator was utilized to record the strain variations for structural deformation assessments. The long-term monitoring results show that this system delivers precise and reliable spatial-temporal measurements about the transverse and longitudinal deformation behavior of bored tunnels during nearby excavations. Zhou et al. (2023) instrumented the sidewalls of several transverse sections in a metro tunnel using optical fiber with a similar method in order to measure the convergence deformation.

In the city center of London, UK, Gue et al. (2015) deployed fiber optic cables to assess the longitudinal deformation behavior of a bored tunnel, constructed by cast-iron segments, when a new tunnel was being constructed nearby. The sensing cable, containing a single-mode *D*-0.9 mm fiber, was prestrained and anchored at specific points along the tunnel vault with a gauge length of 13 m. A BOTDR (with strain accuracy of 3×10^{-5} and spatial resolution of 1 m) was used to collect the strain data. The monitoring results reveal a maximum recorded strain of 1×10^{-4} in tension and 6×10^{-4} in compression.

In addition to structural deformation monitoring, optical fiber was used to develop a leak-detection cable for use in tunnels, by integrating a thin fiber with a super-absorbent polymer jacket (Wang et al., 2023b). The leakage causes expansion of the polymer and subsequently generates strains within the fiber that can be sensed by the interrogator. This leak-detection cable was designed to be installed by point-fixing on sidewalls along the tunnel axis, and its performance was further experimentally checked using an OFDR interrogator.

3.2. Monitoring of NATM tunnels

When constructing a tunnel with the New Austrian Tunneling Method (NATM), the philosophy is to exploit the short-term stability of the surrounding ground by minimizing the disturbance during tunnel face excavation. This is usually achieved via sequential face excavation plus rapid but flexible ground support such as steel mesh grid, arch, and sprayed concrete (or shotcrete) (Karakuş and Fowell, 2004; Thomas, 2019). In NATM tunneling, the front face is typically first divided into multiple small portions and excavated sequentially with a limited step length. As an initial lining, shotcrete is usually sprayed over the exposed surrounding ground after the installation of steel mesh. For the sake of construction safety, it is necessary to monitor the convergence deformation of the shotcrete lining in order to assess the risk of surrounding ground collapse as well as to predict lining damage occurrences. Depending on the ground conditions and function of the tunnel, a secondary permanent concrete lining with reinforcement may be cast on site, and this permanent lining should also be properly monitored during the long-term tunnel operation.

In a transverse cross-section, the concrete lining behaves typically like a curved beam structure and deforms in a flexural mode in response to ground pressures. Similar to the instrumentation of a bored tunnel, the fiber optic cable can be embedded into the lining during construction work (Yao, 2023), preferably on both the inner and outer sides (see Fig. 9), for distributed strain sensing, as shown in De Battista et al. (2015), Sui et al. (2021), Monsberger and Lienhart (2021).

For existing NATM tunnels, distributed strain sensing is usually confined to cables continuously affixed on the inner lining surface, such as for crack development sensing by Grunicke et al. (2021) and Xue et al. (2019). In addition, a fiber optic cable can be installed as a chain of extensometers along the circumferential direction of a transverse section to qualitatively monitor the transverse deformation behavior (oblique and vertical ovalization deformation) such as in Di Murro et al. (2019) and Mohamad et al. (2010), which is similar to monitoring transverse behavior of bored tunnels as in Fig. 6b.

Longitudinally in a NATM tunnel, the ground at the tunnel crown may settle excessively, which implies a danger of collapse disasters, particularly for tunnels in the construction phase with only shotcrete lining and for (coal) mine tunnels without secondary concrete lining. To monitor the settlement behavior of surrounding rocks along a long tunnel longitudinally with conventional geodetic

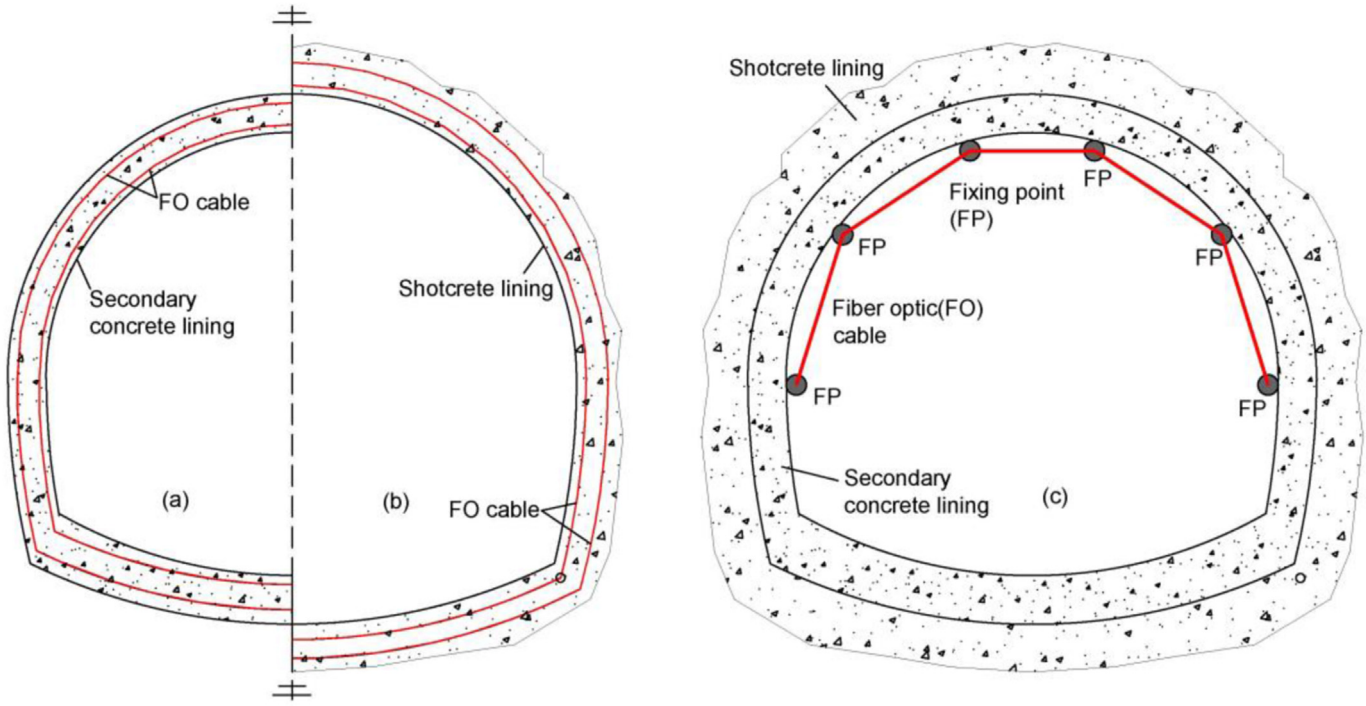

Fig. 9. DFOS instrumentation for transverse deformation behavior monitoring in a NATM tunnel: (a) embedded into the secondary concrete lining and (b) initial shotcrete lining; (c) point-fixing on intrados surface.

measuring (with a total station plus some prisms targets on the tunnel crown) is usually time-consuming and hence will take place with long time intervals only. This might not provide adequate time resolution to warn against imminent collapse. The local settlement of rocks on the roof may induce a longitudinal tensile strain within the shotcrete lining, which can be sensed by a fiber optic cable embedded into it (Monsberger et al., 2022), as shown in Fig. 10a and b. Notably, directly bonding a fiber optic cable continuously on the shotcrete surface is not practical, since the surface is typically very rough, but the cable can be alternatively placed in a slot cut on the surface, as demonstrated by Li et al. (2020). Moreover, the cable can be mounted at discrete locations (along the longitudinal tunnel axis) on the lining surface as illustrated in Fig. 10c, while a differential settlement between two adjacent fixing points can trigger potential strain variations on the gauge length between them (Naruse et al., 2007; Mohamad et al., 2010; Hou et al.,2017, 2019).

(1) Distributed strain sensing

Shi et al. (2005) used optical fibers installed on the lining surface to monitor the deformation of an existing urban road tunnel when a new tunnel was constructed nearby. The single mode *D*-0.9 mm optical fiber was installed by continuous bonding on the lining surface for distributed strain sensing and by point fixing as an extensometer for measuring joint expansion deformation. An additional loose fiber is used for temperature effects compensation and a BOTDR (with a spatial resolution of 1 m and strain accuracy of 4×10^{-5}) is used to collect the data.

In another study (Li et al., 2006), the optical fiber is used to instrument the concrete lining of a NATM tunnel, by continuously bonding on the surface along the tunnel's longitudinal axis, and at the vault on several transverse sections for distributed strain measurement. Similar instrumentation methods have also been employed by Xue et al. (2019), Grunicke et al. (2021), Minardo et al. (2021), and Imai and Mizuno (2020), where the fiber optic cable was used for strain sensing and crack detection in permanent lining, and the study shows that a fiber optic cable bonded on the surface (or into a shallow groove) can monitor concrete strain evolution, and crack widths of submillimeter level using an OFDR interrogator with 1 cm spatial resolution. Additionally, Mao et al. (2011) instrumented several transverse sections of a NATM tunnel by threading the cable through tubes pre-cast into the permanent lining for strain monitoring.

Sui et al. (2021) applied DFOS to monitor the distributed strain at several transverse cross-sections of a NATM tunnel constructed in rock. The fiber optic cable monitored the development of lining deformation during the construction of a closely parallel tunnel. A reinforced cable (Fujikura four-core fiber) was adhered to the inner surface of the concrete lining and at two opposite sides of the temporary steel arch support (made of steel I-beams), whilst a loose-buffered fiber was used for temperature compensation. The DFOS detects the development of cracks on the lining and monitors the vertical and oblique ovalization deformation modes of transverse sections. Strain readings are measured by a BOTDA interrogator with 1 m spatial resolution and strain accuracy of 3×10^{-5}, and the maximum strain sensed was about 7×10^{-4}.

De Battista et al. (2015) embedded the fiber optic cable into the sprayed concrete lining of a NATM tunnel (along both the circumferential and longitudinal directions), to monitor the strain during the excavation of cross-passages in an underground metro station. The cable was fixed at the surface of the initially sprayed shotcrete, and a secondary shotcrete layer was then sprayed to embed the fiber, and a BOTDR with meter-order spatial resolution collected the data. Li et al. (2020) also embedded the fiber optic cable into the shotcrete lining but used a continuous shallow groove cut in the surface. The cable was installed in both longitudinal and circumferential directions in the primary shotcrete layer and used to monitor the deformation during the subsequent tunneling process with a BOTDR of 1 m spatial resolution.

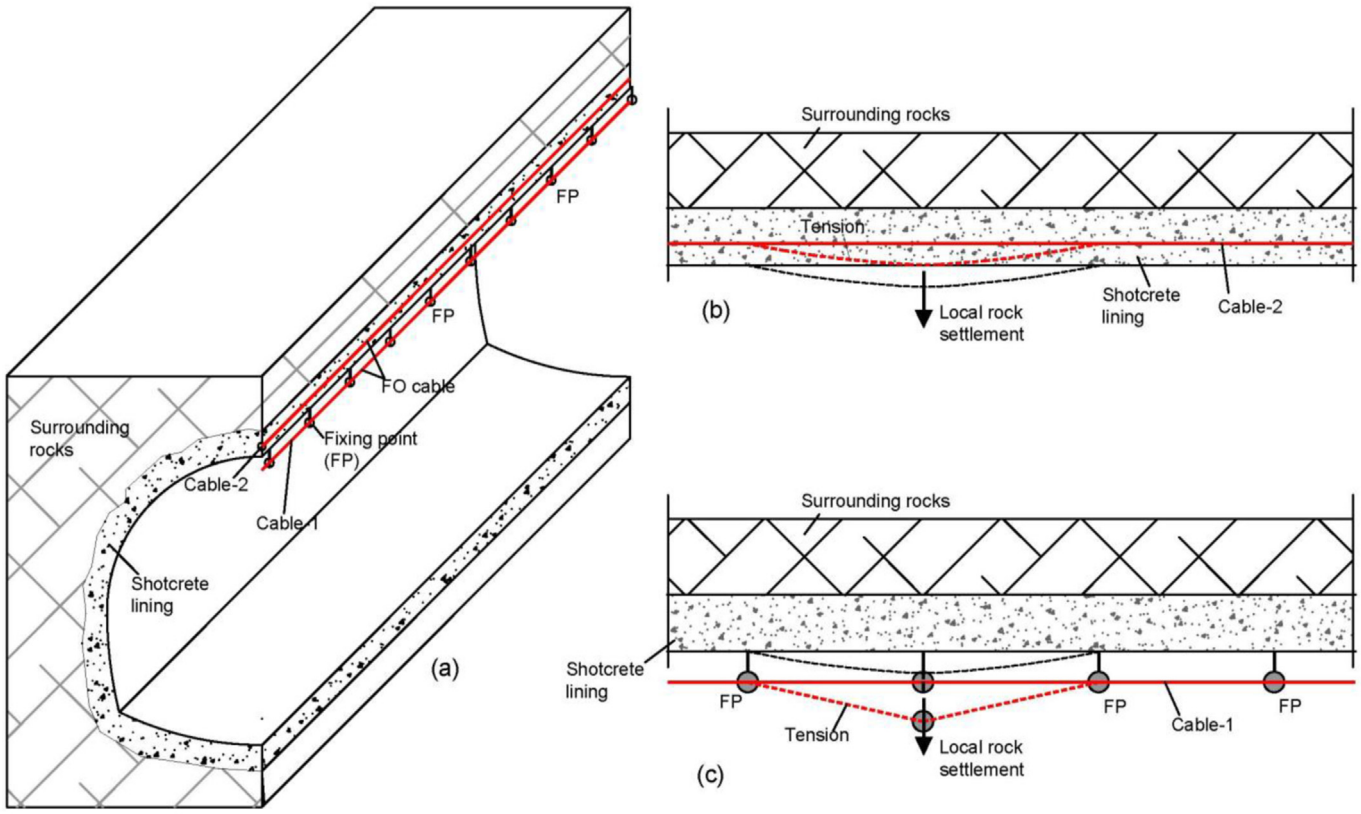

Fig. 10. Fiber optic cable instrumented longitudinally for rock settlement measuring: (a) overall layout; (b) fiber embedding into the lining and (c) point-fixing on the surface.

Wagner et al. (2020) instrumented the initial shotcrete lining of several cross-sections in the Semmering Base Tunnel with two layers of embedded fiber optic cable. The strain information was sampled via an OFDR system typed OBR4600 with a 2 cm spatial resolution. The strain distribution was further used to analyze the flexural curvature of the shotcrete lining in Monsberger and Lienhart (2021). In a similar study by Monsberger et al. (2022), the fiber optic cable was embedded to instrument both the initial shotcrete (single fiber layer) and the secondary concrete linings (double fiber layers) for distributed strain sensing. It was confirmed that the DFOS can overcome the limitations of point-wise sensors and provide continuous strain profile information for a more comprehensive examination of tunnel lining behavior.

In addition to distributed sensing in field monitoring, DOFS is also used for strain sensing in laboratory-scale experiments of tunneling construction (Liu et al., 2017; Zhu et al., 2020). For example, Liu et al. (2017) embedded the *D*-0.9 mm optical fiber into the ground surrounding the tunneling face, both along the longitudinal tunnel axis and in transverse directions (perpendicular to the tunnel axis), to measure strain developed within the ground during the sequential face excavation process, and an OFDR of cm-order resolution collected densely distributed strain information for a ground response analysis.

(2) Extensometer use for point displacement monitoring

Mohamad et al. (2010) applied DFOS to examine the deformation behavior of an old masonry tunnel while constructing a new tunnel beneath it (with a minimum clearance of 3.6 m). Optical fibers attached along the intrados surface by point-fixing (with a gauge length of around 1.4 m) at five transverse sections recorded the relative strains of tunnel deformation between the fixed points. Besides, the fiber is also installed longitudinally along the springlines and crown by point-fixing, to monitor the flexural behavior along the longitudinal tunnel axis. A *D*-0.9 mm single-mode fiber was adopted as the sensing fiber, with a *D*-6.9 mm loose-buffer fiber used for temperature effects compensation. A BOTDR type AQ8603 (1 m spatial resolution, strain accuracy of 4×10^{-5}) was used to record the strain. The sensing fiber was imposed a prestrain of 0.2%–0.3% before being point-glued at the steel hooks that are plugged into the lining.

A similar monitoring study was conducted by Acikgoz et al. (2017) on a historic brick barrel vault during nearby piling construction, where the optical fiber is installed as extensometers with the same "hook and pulley" method as in Mohamad et al. (2012). They show that the deformation behavior inferred from DFOS strain readings agrees with the results assessed from total station monitoring. In the studies by Di Murro et al. (2019) and Hou et al. (2021), the optical fiber instrumented several cross-sections on the intrados lining surface of a NATM tunnel in rock for distortion monitoring. Schenato et al. (2016) installed the fiber optic cable as extensometers spanning cracks observed on the lining surface for monitoring the crack width variations.

For monitoring the longitudinal mine cavity deformation behavior, Naruse et al. (2007) placed the fiber optic cable as extensometers along the longitudinal axis on the sidewall and vault by point fixing, to monitor the deformation status of an underground mine cavity (as illustrated in Fig. 10c). The relative deformation between two adjacent fixed points causes a strain variation within the gauge length that can be potentially measured by the interrogator (a BOTDR of 2 m in this case). In a similar study conducted by Hou et al. (2017), the optical fiber is designed to be fixed at discrete spots on the roof of a coal mine along the longitudinal axis, to measure the rock mass settlement, and laboratory

experiment shows that fiber strain readings can help to quantitatively infer the settlement.

Moffat et al. (2015) developed a special PVC tube with integrated optical fiber to measure the rock mass movement in an underground mine tunnel (with only shotcrete lining). The single-mode *D*-0.9 mm optical fiber is glued continuously along four lines of the tube surface which are oriented 90° from each other using epoxy glue, to capture in-plane and out-of-plane tube bending displacements (see Fig. 11). The fiber was applied an initial tensile strain of about 0.1%, and a BOTDR apparatus was used to measure fiber strain. The optical fiber measures longitudinal strains caused by pipe bending deformation induced by the relative settlements of its anchorage supports (rigidly connected to the rock mass). Laboratory experiments validated the applicability of this pipe sensor and it was subsequently deployed for field monitoring.

3.3. Monitoring of immersed tunnels

Immersed tunnels have been built in many places worldwide as fixed links beneath waterways. The construction of an immersed tunnel typically starts by fabricating a number of short tunnel segments which are further assembled into longer elements (usually around 100 m) in a dry dock. The elements are successively transported to the tunnel site and immersed in a prepared trench on the riverbed (Lunniss and Baber, 2013). Longitudinally, an immersed tunnel behaves like a chain of jointed segments set on a prepared foundation. Two types of joints exist within a segmented immersed tunnel, namely immersion joints and dilation joints (as indicated in Fig. 12a). Immersion joints are formed when elements are immersed and connected under the water, whereas dilation joints are formed when the elements are manufactured segment by segment in a dry dock.

During the long service period, excessive joint deformations (shown in Fig. 12b), primarily the opening and closing longitudinally and differential settlements (of the two sides at a joint) vertically, may deteriorate the tunnel's structural integrity, crack the concrete locally at joints and trigger leakages (Gavin et al., 2019; Wang et al., 2020; Zhang et al., 2021). Therefore, for a thorough assessment of the structural health, the joint deformations along the whole length of the tunnel should be monitored properly.

Zhang and Broere (2023a, b) developed a joint deformation monitoring system for immersed tunnels using DFOS. At each joint, the fiber optic cable is installed to form a sensor block that is composed of two extensometers spanning the joint gap (see two gauge lengths GL1 and GL2 fixed at three fixing points FP1 to FP3 in Fig. 13), and this allows for simultaneous measurement of both horizontal joint opening and vertical uneven settlement over the immersion and dilation joints. For a field application in the First Heinenoordtunnel in the Netherlands, the installed DFOS system has been shown to detect sub-millimeter joint deformations and conduct measurements at sub-hour or better intervals without interfering with the regular tunnel operation.

3.4. Monitoring of cut-and-cover tunnels

The cut-and-cover tunneling method is typically used to build relatively shallow tunnels, where an excavation is first made from the surface to the designated depth. The tunnel structure is then constructed on site, followed by backfilling (Chapman et al., 2017). The cut-and-cover method is especially suited for constructing underpasses for traffic use and utility tunnels. Structurally, cut-cover tunnels mostly have a rectangular cross-section and can be divided into separate units (or elements) longitudinally, with special embedded rubber gaskets to seal the construction joints. The cut-and-cover tunnel usually behaves similarly to an immersed tunnel, and optical fiber can be adopted to measure the distributed strain when continuously glued on the tunnel structure, as well as to observe the localized deformations at the joints.

Cui et al. (2021b) glued a *D*-0.9 mm fiber continuously on the internal surface (embedded into a small slot cut into the concrete) of a shallow utility tunnel and measured its deformation behavior when a new bored tunnel was constructed beneath it. Overall, the DOFS demonstrated good technical performance for use in cut-and-cover tunnel structure monitoring, similar to the use in immersed tunnels.

4. Discussion on practical aspects in DFOS monitoring

The previous studies reviewed above have validated the applicability of distributed fiber optic sensors (DFOS) in monitoring underground tunnel infrastructure, where the DFOSs were flexibly instrumented for distributed strain sensing and point displacement measuring. The essential information on DFOS applications in typical literature is further summarized in Table 2. This section presents an in-depth discussion of the three key aspects of practical DFOS monitoring: the proper sensing fiber selection, the effective sensing layout design, and the establishment of robust field sensor instrumentation.

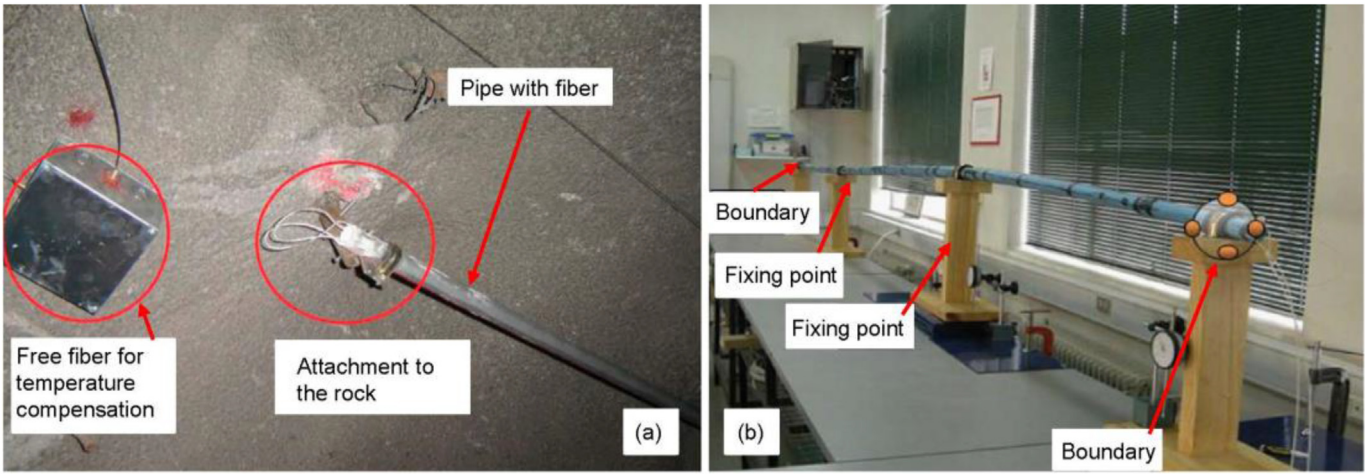

Fig. 11. Host-pipe with optical fiber for tunnel wall settlement measuring: (a) field installation and (b) laboratory validation (Moffat et al., 2015).

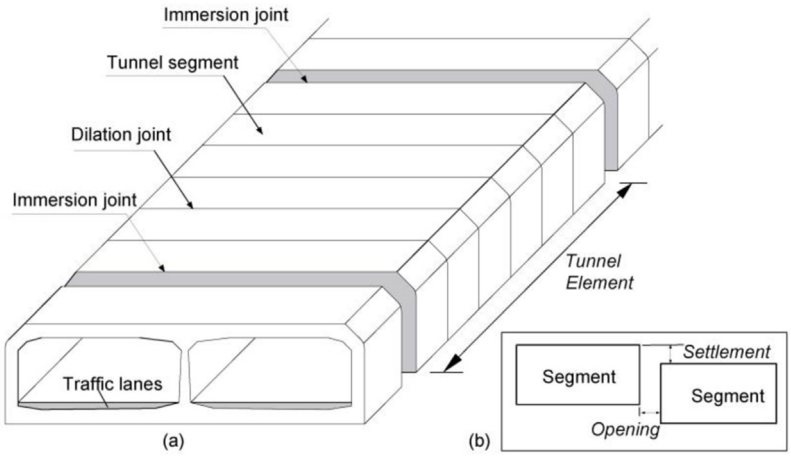

Fig. 12. Schematic of (a) a segmented immersed tunnel structure and (b) joint deformations.

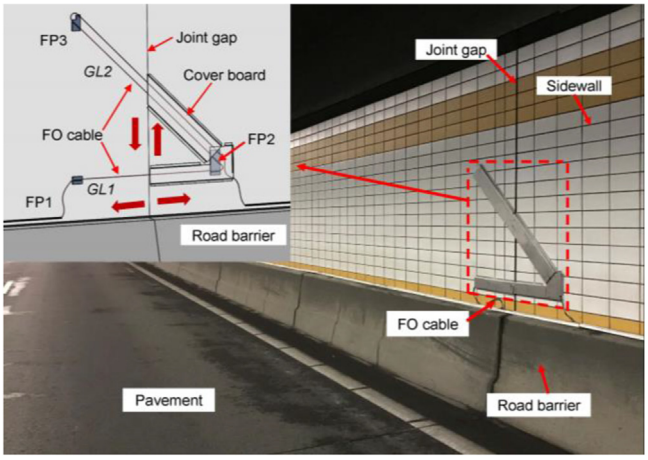

Fig. 13. Monitoring immersed tunnel joint deformation using DFOS in the Heinenoordtunnel.

4.1. Sensing fiber selection of bored tunnels

This section assesses optimal fiber selection and its suitability for practical monitoring. Fig. 14 depicts the optical fiber/cable types deployed in current literature, ranging from small ordinary *D*-0.9 mm fiber to highly metal-reinforced sensing cable products. The selection of a qualified sensing fiber should be based on, first and foremost, the anticipated harshness of the working conditions and the possibility of fiber repair in case of breakage. For instance, fiber optic cables directly embedded in the concrete lining during the construction stage generally require a higher grade of protection, as they are more susceptible to damage during the installation process and are hardly able to be accessed, replaced, and repaired afterwards, compared to fibers attached to the intrados surface of the tunnel after construction.

The *D*-0.9 mm tight-buffer fiber, typical with a diameter of core/cladding/jacket of 9 μm/125 μm/900 μm and shown in Figs. 2b and 14a, is very thin and has a low axial stiffness that can be easily prestrained at installation. The *D*-0.9 mm fiber made for ordinary applications in the telecommunications industry will have a maximum working strain (MWS) level of around 0.6%, but for some dedicated sensing fibers, the MWS can be more than 1% (Zhang and Broere, 2022). Due to its relatively limited resistance to external impacts, this fiber type is not typically suggested for long-term field monitoring, but it is highly suitable for laboratory experimental studies (Liu et al., 2017; Guo et al., 2023; Yang et al., 2023). In previous studies, this *D*-0.9 mm fiber was prestrained and then continuously glued (for distributed strain sensing) or spot-fixed (for extensometer use) on the tunnel intrados surface in field monitoring (Shi et al., 2005; Mohamad et al., 2010; Gue et al., 2015; Acikgoz et al., 2017), but it should be noted that these instrumented tunnels are either out of service or not highly accessible to the general public, which implies that the potential for undesired impacts on the fiber is estimated as low to insignificant.

A polyurethane-coated *D*-2 mm fiber optic cable (type NZS-DSS-C07 from Nanzee Sensing (2022)) with a single core, as depicted in Figs. 2c and 14b, is mostly manufactured from the primary *D*-0.9 mm fiber by adding a tight-buffered thick polymer jacket externally and was used in Zhu et al. (2022) and Zhang and Broere (2023a). Compared with the *D*-0.9 mm fiber, this fiber type is given more protection by the thicker jacket and is therefore more robust to external impacts when handling. Moreover, note that the pure polymer jacket only provides a limited strengthening effect (compared with metal reinforcement) and therefore this fiber type still has a moderate stiffness that can be prestrained easily by hand, for instance, to a strain level of 0.5% as in Zhu et al. (2022). Consequently, this type of polyurethane-coated *D*-2 mm fiber is a suitable alternative to the *D*-0.9 mm fiber, whether in the case of spot-fixing for extensometer use as in Mohamad et al. (2012) and Acikgoz et al. (2017) or continuously bonding on the lining surface as in Wang et al. (2023a) for distributed strain sensing.

To further boost the protection level, a reinforced fiber optic cable with single or multiple cores usually integrates reinforcement parts into the fiber cross-section, using metal tubes as in Fig. 14e and g, metal reinforcement strings or wires as in Fig. 14c–f, and g (Nanzee Sensing, 2022; Solifos AG, 2023), or glass fiber reinforced polymer (GFRP) reinforcement (Nanzee Sensing, 2022; Wang et al., 2023a) as illustrated in Fig. 14d. The reinforcement assures the high robustness of the cable and makes it suitable for use in very harsh monitoring environments, such as being buried in the concrete lining. However, the high axial stiffness that results from the reinforcement parts may pose an obstacle to manual prestraining and fiber anchorage. According to previous studies utilizing the reinforced fiber optic cable (as listed in Table 2), the prestraining level at field installation is mostly below 0.2%, such as in De Battista et al. (2015), and the observed strain lies within the range of 0.1%, which implies the prestraining of these reinforced cables to a low strain level is still achievable without too much difficulty. Finally, a reinforced fiber optic cable with multiple cores (as in Fig. 14c) has

Table 2
A summary of essential DFOS application information in previous studies.

Tunnel type	Source	Interrogator type	Spatial resolution (m)	Instrumented structure parts	Measurand	Installation method (L is gauge length)	Temperature compensation	Sensing fiber type	Pre-straining	Maximum sensed strain
Bored tunnel	Cheung et al. (2010)	BOTDR	1	Intrados surface	Point displacement	Point fixing, $L = 0.6$ m	Loose-buffer cable	D-0.9 mm fiber	About 0.35%	
	Wang et al. (2013)	BOTDA	0.1	Intrados surface (scaled laboratory test)	Point displacement	Point fixing, $L = 0.8$ m	Slack fiber section	Reinforced ribbon cable (5.2 mm × 1.2 mm)	About 0.3%	0%; 1.2%
	Mohamad et al. (2012)	BOTDR	1	Intrados surface	Point displacement	Point fixing, $L = 1.12$ m	Loose-buffer cable	D-0.9 mm fiber	0.15%	−0.063%; 0.035%
	Gue et al. (2015)	BOTDR	1	Intrados surface (with cast-iron segments)	Distributed strain and point displacement	Overall bonding and point fixing, $L = 13$ m	Slack fiber section	D-0.9 mm fiber	0.1% −0.3%	−0.06%; 0.055%
	Wang et al. (2018)	BOFDA	0.2	Intrados surface	Point displacement	Point fixing, $L = 1.2$ m	Slack fiber section	D-2 mm cable	0.5%	−0.33%; 0.03%
	Seo et al. (2017)	BOTDR	1	Inside concrete lining	Distributed strain	Embedded into the concrete segment	Loose-buffer cable	Reinforced ribbon cable (5.2 mm × 1.2 mm)	0%	−0.04%; 0.02%
	Monsberger et al. (2018)	OFDR (OBR 4600)	0.02	Inside concrete lining	Distributed strain	Embedded into the segment		Reinforced cable (V9 type D-3.2 mm)	0%	0%; 0.6%
	Gómez et al. (2020)	OFDR (OBR ODiSI-A)	0.01	Intrados surface	Distributed strain	Overall bonding on the surface				−0.015%; 0.015%
	Sui et al. (2022)	BOTDR	1	Inside concrete lining	Distributed strain	Embedded into the concrete segment	Loose-buffer cable	Reinforced ribbon cable (5.2 mm × 1.2 mm)		−0.04%; 0.015%
	Hong et al. (2022)	OFDR	0.001	Inside concrete lining (extrados)	Distributed strain	Embedded into the concrete segment		Metal-reinforcement cable		−0.03%; 0.005%
	Zhu et al. (2022)	BOFDA	0.2	Intrados surface	Point displacement	Point fixing, $L = 1$ m, and 1.2 m	Slack fiber section	D-2 mm tight-buffer cable	0.5%	−0.085%; 0.87%
	Wang et al. (2023a)	BOFDA	0.2	Inside filling concrete; Core steel tube;	Distributed strain	Embedded into the concrete; Overall bonding on the outer surface of steel tube		Metal-reinforcement cable; D-2 mm tight-buffer cable	0%	−0.0108%; 0.064%
	Zhang et al. (2022b)	OFDR (OBR 4600)	0.01	Inside concrete lining; concrete surface (laboratory test)	Distributed strain	Embedded into the concrete; Overall bonding on the outer surface		D-0.9 mm fiber		−0.9%; 0.4%
	Yang et al. (2023)	BOFDA	0.1	Intrados surface (scaled laboratory test)	Distributed strain	Overall bonding on the intrados surface;	Slack fiber section	D-0.9 mm fiber	0%	−0.005%; 0.03%
	Guo et al. (2023)	OFDR (OBR 4600)	0.01	Inside concrete lining; concrete surface (laboratory test)	Distributed strain	Embedded into the concrete; Overall bonding on the outer surface		D-0.9 mm fiber		−0.1%; About 1.3%
	Jiao and Zhou (2021)	BOTDA	0.15	Intrados surface (scaled laboratory test)	Distributed strain	Overall bonding on the intrados surface	Slack fiber section			0%; 0.11%
NATM tunnel	Shi et al. (2005)	BOTDR	1	Concrete lining surface	Distributed strain and point displacement	Overall surface bonding and point fixing, $L = 1.2$ m	Slack fiber section	D-0.9 mm fiber		
	Naruse et al. (2007)	BOTDR	2	Internal surface of a mining cavity	Point displacement	Point fixing, $L = 3$ m	Loose-buffer cable		About 0.23%	
	De Battista et al. (2015)	BOTDR	1	Inside shotcrete lining	Distributed strain	Embedded into shotcrete lining	Loose-buffer cable	Reinforced ribbon cable (5.2 mm × 1.2 mm)	0.1%	−0.082%; 0.0567%
	Sui et al. (2021)	BOTDR	1	Permanent concrete lining surface; steel girds	Distributed strain	Overall bonding on the surface	Loose-buffer cable	Reinforced ribbon cable (5.2 mm × 1.2 mm)		−0.07%; 0.03%
	Mohamad et al. (2010)	BOTDR	1	Intrados surface (Masonry-lined Tunnel)	Point displacement	Point fixing, $L = 1.4$ m	Loose-buffer cable	D-0.9 mm fiber	0.2% −0.3%	−0.08%; 0.16%
	Moffat et al. (2015)	BOTDR		rock mass settlement on a mining cavity	Distributed strain sensing	Overall bonding on the host pipe surface	Slack fiber section (in field use)	D-0.9 mm fiber	0.1%	−0.08%; 0.08%
	Hou et al. (2017)	BOTDR		Internal surface of a mine vault	Point displacement	Point fixing, $L = 4$ m/5 m/6 m		D-0.9 mm fiber	0%	0%; 0.12%
	Acikgoz et al. (2017)	BOTDR	1	Intrados surface (Brick barrel vaults)	Point displacement	Point fixing, $L = 2$ m	Slack fiber section	D-0.9 mm fiber		−0.025%; 0.09%
	Liu et al. (2017)	OFDR (OBR 4600)	0.005	Inside surrounding ground (scaled laboratory test)	Distributed strain	Embedded into soils		D-0.9 mm fiber		0%; 0.035%
	Xue et al. (2019)	BOTDR	1	Intrados surface (permanent lining)	Distributed strain	Overall bonding on the surface	Loose-buffer cable	D-2 mm fiber		0%; 0.15%

Table 2 (*continued*)

Tunnel type	Source	Interrogator type	Spatial resolution (m)	Instrumented structure parts	Measurand	Installation method (*L* is gauge length)	Temperature compensation	Sensing fiber type	Pre-straining	Maximum sensed strain
	Di Murro et al. (2019)	BOTDA	1	Intrados surface	Point displacement	Point fixing, *L* about 1 m	Slack fiber section	*D*-0.9 mm fiber		−0.03%; 0.03%
	Wagner et al. (2020)	OFDR (OBR 4600)	0.002	Inside shotcrete lining	Distributed strain	Embedded into lining	Loose-buffer cable	Reinforced cable (V3 type *D*-7.2 mm)		−0.156%; 0.02%
	Li et al. (2020)	BOTDR	1	Intrados surface (permanent lining)	Distributed strain	Overall bonding on the surface		Metal reinforced cable		0%; 0.01%
	Minardo et al. (2021)	BOTDA	1	Intrados surface (permanent lining)	Distributed strain	Overall bonding on the surface		*D*-0.9 mm fiber		0%; 0.4%
	Grunicke et al. (2021)	OFDR (OBR 4600)	0.01	Intrados surface	Distributed strain	Overall bonding on the surface	Other temperature sensors			−0.1%; 0.15%
	Hou et al. (2021)	BOFDA	0.2	Intrados surface (scaled laboratory test)	Point displacement	Point fixing, *L* about 0.48 m	Slack fiber section	*D*-0.9 mm fiber		−0.55%; 0.7%
	Monsberger et al. (2022)	BOFDA	0.5	Inside shotcrete lining and Permanent concrete lining	Distributed strain	Embedded into lining	Loose-buffer cable	Reinforced cable (V3 type *D*-7.2 mm; V9 type *D*-3.2 mm)		−0.05%; 0.02%
Immersed tunnel	Zhang and Broere (2023a)	BOFDA	0.2	Sidewall surface	Point displacement	Point fixing, *L* = 0.8 m/1.27 m/ 1.35 m/1.91 m	Slack fiber section	*D*-2 mm cable	0.5%	−0.5%; 0.6%
Cut-cover tunnel	Cui et al. (2021b)			Intrados surface	Distributed strain	Overall bonding on the surface		*D*-0.9 mm fiber	0%	0%; 0.006%

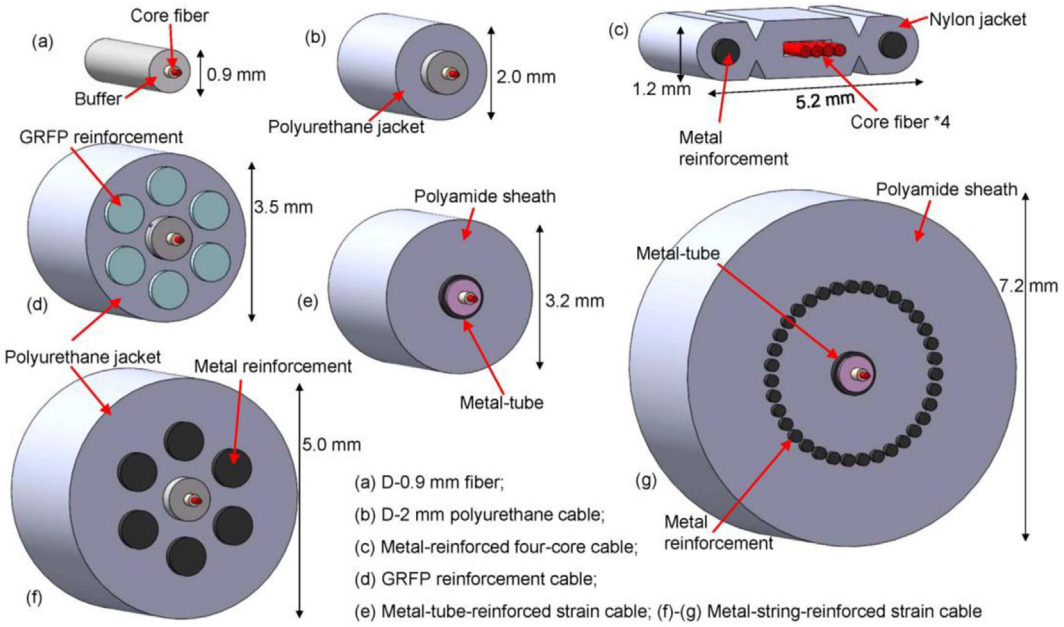

Fig. 14. Illustration of strain sensing fiber types used in the literature.

the advantage of offering multiple measuring channels (Seo et al., 2017), and this is especially advantageous when utilizing different types of interrogators (with different plug types) simultaneously, or when measuring temperature effects using interrogators based on (only temperature-related) Raman scattering.

In addition, a loose-buffered fiber optic cable is often used for temperature effects compensation. When buried into the structure, a loose-buffered fiber with a stiff jacket is preferred, whereas for surface instrumentation, both tight-buffered (installed without mechanical strain) and loose-buffered cables can be adopted. More discussion on this topic is presented in Section 4.3 on temperature effects compensation.

Finally, in some field monitoring applications, a connection cable may be necessary when the interrogator is positioned at a distance from the instrumented locations. A connection cable is preferably a highly reinforced cable with multiple cores. As long as the fiber core and cladding of the fiber are the same size as the sensing fiber, they can be fusing-spliced conveniently. Connection cables can be ordinary fiber optic cables available from the telecommunication industry, as they are often less expensive than dedicated strain-sensing cables.

4.2. Sensor layout design

Generally, an effective sensing layout design should take into account: the range of sensing strain, an explicit transfer relation (or sensing mechanisms) from fiber strain to the target observable (displacement, flexural deflection, etc.), and ease of field sensor installation.

For distributed strain sensing, the fiber is continuously glued on the surface or embedded into the host material, typically the concrete. In this application, the sensor layout is relatively simple, but the key is to install the fiber properly while, in most cases, imposing a designated prestrain level on the fiber. Generally, a prestrain level of 0.1%–0.2% is seen in most previous studies when monitoring concrete structures. More discussion on reliable fiber prestraining is presented in Section 4.3 on field sensor instrumentation. Additionally, the strain transfer effects between the host matrix and the optical fiber determine the sensing performance. According to Hou et al. (2020), for a fiber continuously bonded to concrete, full strain transfer can be reached along the vast middle lengths in normal monitoring conditions, while only at the two short fiber ends a partial strain transfer is achieved, and these boundary effects generally impose negligible effects on the overall distributed strain sensing results. In addition, an initial calibration helps to identify the influence length of these boundary effects and can locate the weak strain transfer sections along the sensing fiber.

In most monitoring studies the distributed strain directly sensed by the fiber serves as an explicit indicator for assessing the tunnel lining deformation behavior or cracking risks (Xue et al., 2019; Grunicke et al., 2021; Hong et al., 2022). However, in some monitoring studies, the strain information is further analyzed to infer the lining convergence (or shape), where the tunnel lining is usually assumed to behave as a curved beam under flexural (or combined flexural-axial) deformation patterns, such as in Mohamad et al. (2012), Sui et al. (2021) and Monsberger and Lienhart (2021).

For extensometer use, the sensor layout design must take into account additional factors. When designing a fiber optic extensometer, the gauge length, the necessity and the amount of fiber pre-straining, and the point fixing method (by glue or special clamps) should all be considered. In most studies, the gauge length is usually taken as longer than the spatial resolution of the interrogator, so that the systematic error resulting from spatial resolution can theoretically be eliminated. Moreover, the prestraining level of the gauge length can reach 0.5% or even higher as in Zhu et al. (2022) and Zhang and Broere (2023a), since insufficient initial tensile strain would cause the fiber to sag under compressive deformation.

When the fiber is used as an extensometer for relative displacement measurements (between the two fixed points), such as in monitoring tunnel joint opening explicitly, the axis of the gauge length should be aligned with the direction of deformation (say, perpendicular to the joint gap), in order to maintain a high strain sensitivity to the measured deformation. Taking the single fiber optic extensometer shown in Fig. 15 for example, a gauge length of L_0 is determined by both ends P_1 and P_2 fixed on the structure surface. For simplicity, only in-plane point displacements Δx and Δy are analyzed. Assuming relative displacements occur that displaces P_2 to P_2', the mathematical relation between point displacements and fiber strain ε is expressed as

$$\frac{\sqrt{(L_0+\Delta x)^2+\Delta y^2}-L_0}{L_0}=\varepsilon \tag{3}$$

From Eq. (3), it can be derived that

$$1+\frac{2\Delta x}{L_0}+\left(\frac{\Delta x}{L_0}\right)^2+\left(\frac{\Delta y}{L_0}\right)^2=(1+\varepsilon)^2 \tag{4}$$

Theoretically, a single gauge length cannot accurately sense both displacement components Δx and Δy, unless an additional extensometer is added, such as in Zhang and Broere (2023a). If the gauge length is set to 1 m (which appears the case in most studies), it can be inferred that the current sensor layout is much more sensitive to the horizontal displacement Δx, and the effects of vertical displacement Δy on the fiber strain are so insignificant as to be negligible. For instance, a vertical displacement of 20 mm only triggers a strain of 1×10^{-5} within the fiber that most interrogators can hardly detect. Therefore, this validates the rationality of the simplification in the sensing principle that the gauge length spanning the tunnel joint gap is capable of measuring joint opening with adequate accuracy, while the potential effects of vertical relative settlement at the joint are negligible, as described in Wang et al. (2018), Zhu et al. (2022) and Zhang and Broere (2023a).

Moreover, the sensitivity analysis above implies that a horizontally aligned extensometer does not have a high sensitivity for measuring a relative vertical displacement. For instance, in the study by Naruse et al. (2007) and Hou et al. (2017), the horizontal fiber optic extensometers are designed to measure the relative settlement of two adjoining fixed points on a mine vault, see Fig. 16. This sensor layout is more applicable for measuring large-scale settlements, as it can be inferred that a significant settlement of 10 cm only causes a strain of 5×10^{-5} (with a gauge length of 1 m), which is hard to accurately distinguish by the interrogator. An alternative sensor layout to improve the sensor sensitivity is studied by Moffat et al. (2015), where the fiber optic cable is first continuously glued on the surface of a host pipe that is anchored to the mine tunnel vault at discrete points, as shown in Fig. 16. The relative settlement then triggers a significant flexural strain within the pipe which can be efficiently sensed by the surface-glued cable, and therefore this sensor layout can enhance the cable strain sensitivity to the desired observable.

If both displacement components Δx and Δy are desired to be measured simultaneously, for instance, the joint opening and relative settlement (of the two sides of a joint), an additional extensometer is required, as in the study by Zhang and Broere (2023b) where two extensometers are combined to form a sensor block, as depicted in Fig. 13. The horizontal extensometer is dedicated to measuring the joint opening, and by deducting the joint opening effects from the strain readings of the inclined one, the relative settlement can be calculated. Moreover, the angle of the inclined fiber influences its sensitivity to the vertical settlement, since a larger angle corresponds to a higher sensitivity. A final fiber layout design will have to consider the tunnel joint's physical dimensions and the ease of field instrumentation.

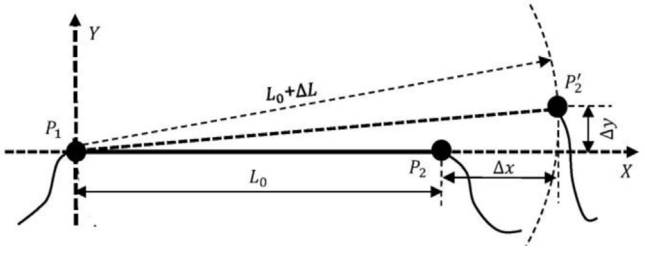

Fig. 15. Deformation pattern occurring on the fiber optic extensometer.

4.3. Field sensor instrumentation

A precise but practical field sensor instrumentation scheme is critical to achieve monitoring quality. Both fiber selection and

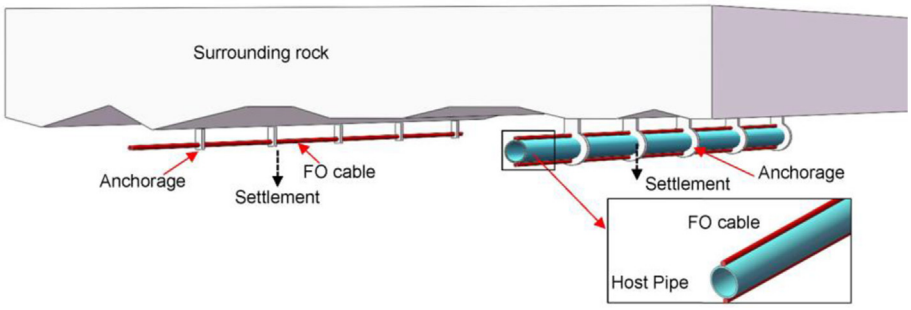

Fig. 16. Measuring rock mass settlement in underground mining cavities (left-direct fiber anchorage method; right-host pipe method).

fixing methods should be specified when designing the field instrumentation scheme. The optimal sensing fiber selection has to take into account the observables (distributed strain or point displacements), the fiber's working environment, and the ease of prestraining (axial stiffness), whereas the fiber anchorage method is usually determined by the level of fiber prestraining and the physical conditions (such as the surface smoothness, curved or flat surface) of the host structure.

(1) For distributed strain sensing

For distributed strain sensing inside the tunnel lining, the fiber optic cable is typically installed at the time of tunnel construction. In such monitoring applications, the fiber must firstly survive the potential external impacts, often caused by shotcrete spraying and vibration in concreting, and secondly, be installed in a way to deform consistently with the concrete. Therefore, in previous studies, the sensing cables selected for burial into the lining are mostly reinforced cables with single or multiple cores, such as in Fig. 14c–g.

For monitoring of a NATM tunnel such as by Wagner et al. (2020), Monsberger and Lienhart (2021), and Hruby et al. (2019), the fiber optic cable can be first secured to the steel mesh or girder with clamps or fastening ties, and a subsequent shotcrete layer will embed the fiber inside the initial lining for strain sensing. When instrumenting the secondary permanent concrete lining, the fiber is also initially attached to the reinforcement bars in the section before concrete pouring. Note that when directly bonding the fiber optic cable continuously on the lining surface, a small slot can be cut at the surface and the sensing fiber can then be buried inside, after which the slot is filled with glue or mortar, such as in Xue et al. (2019), Li et al. (2020) and Minardo et al. (2021).

For monitoring the flexural behavior of bored tunnels, the tunnel segments are instrumented by embedding fibers beforehand, such as described in Seo et al. (2017), Sui et al. (2022), Monsberger et al. (2018) and Hong et al. (2022). Generally, each individual segment is instrumented with an independent fiber section, while the two fiber ends are extended externally and subsequently connected to the fiber sections within the neighboring segments once all segments are assembled on site, as depicted in Fig. 17. In the fiber optic cable-segment integration, the cable was first attached to the reinforcement cage, at the intrados and extrados of the segment, before being placed into the steel module for subsequent concreting, as shown in Fig. 17c. Note that aligning the fiber axis exactly following the curved rebar (along the circumferential direction) while, at the same time, imposing a prestrain, is not as easy as aligning it in a straight line (such as when placed in the longitudinal direction of the tunnel). However, according to the study by Seo et al. (2017), an unstrained fiber buried into the concrete may

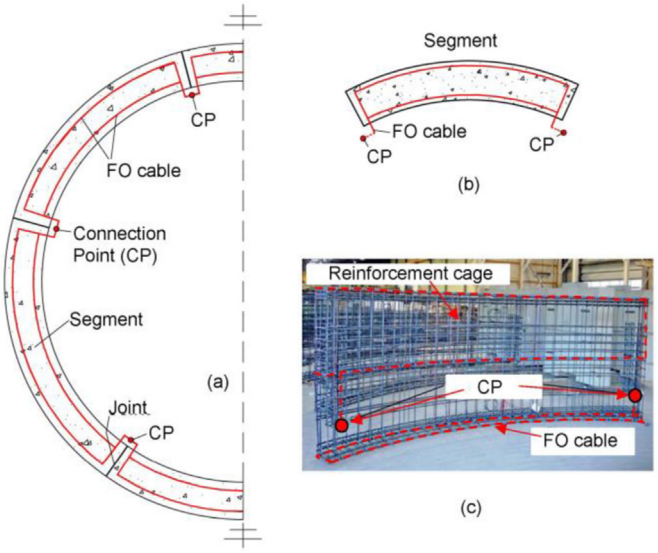

Fig. 17. Fiber optic instrumentation route in (a) segment ring, (b) single segment, and (c) reinforcement cage (Monsberger et al., 2018).

still detect compressive strains in the segment. Moreover, applying a small level of prestrain (for example, 0.1%) in such a curved fiber line is possible, as shown by Sui et al. (2022), and sufficient since in most distributed strain monitoring, the measured compression is below 0.1%. Last but not least, sufficient protection of the fiber ends is critical for successful instrumentation, as damage to fiber ends may easily occur during the construction process, such as the breakage reported by Seo et al. (2017) and Sui et al. (2022).

The procedure of attaching the fiber optic cable to the reinforcement cage may vary for different instrumentation conditions. The cable can be conveniently secured to the reinforcement at discrete points, with portable clamps as demonstrated in Fig. 18c, such as a wire clamp with nuts and plastic fasteners (or ties). It should be noted that adjustable physical clamps with nuts will result in significant squeezing forces on the outer jacket of the fiber, and therefore these clamps are more suitable for reinforced cables which can withstand large squeezing forces. Compared to these adjustable physical clamps, fixing the fiber with glue such as epoxy glue is gentler on the fiber, but the required hardening time of the glue may impose some limitations to field instrumentation: on one hand, it may require more handling time which is difficult to guarantee on a complex construction site; on the other hand, the glue may not sustain the initially imposed prestrain (if needed) within the fiber. Therefore, when attaching the fiber optic cable on a construction site like in a NATM tunnel project, physical clamps

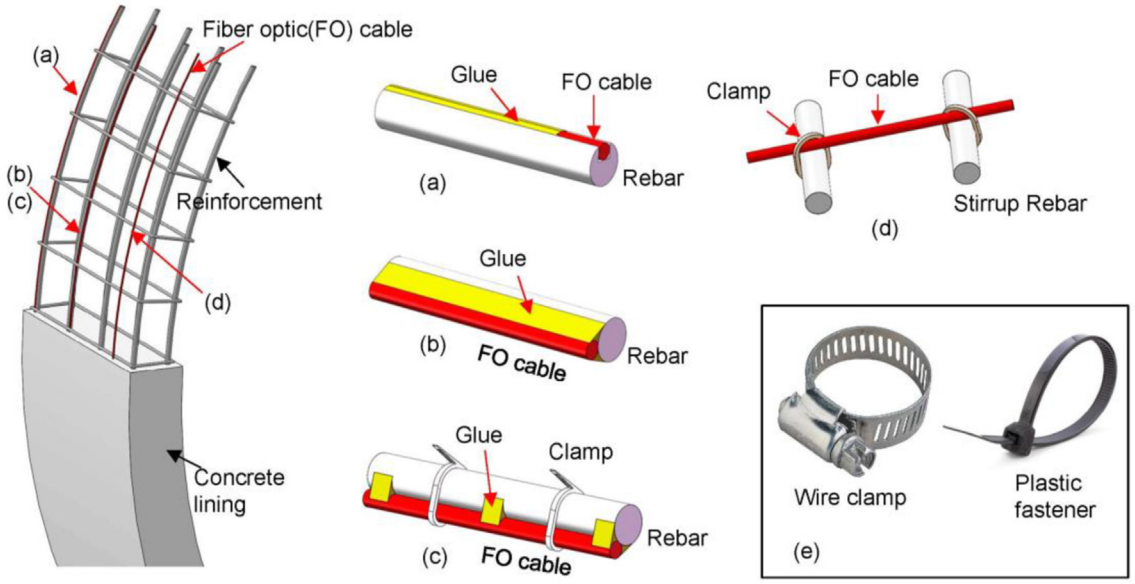

Fig. 18. FO cable-rebar integration: (a) embedding into a shallow slot; (b) surface continuous bonding; (c) point fixing with glue and clamps; (d) point fixing with physical clamps; (e) physical clamp for fiber fixing.

are more commonly adopted as described in Wagner et al. (2020); however instrumenting the individual segments (of bored tunnels) is conducted indoors, typically in the segment manufacturing factory, and it gives more time for handling which allows for continuously bonding or discrete point bonding to the rebar such as in Fig. 18b and c, with the initial aid of physical clamps.

Another possible way to reduce the fiber installation difficulty (on curved rebar) is to firstly cut a small slot on the rebar that serves as a laying channel for the fiber optic cable, and the fiber can be bonded by filling the slot gap with glue (Guo et al., 2023), as shown in Fig. 18a. However, this will require additional slot-cutting work on the rebar, which is more likely confined to instrumenting a limited number of segments in an indoor environment. Finally, when instrumenting the tunnel lining for flexural behavior monitoring, the fiber optic cable route is preferred to closely align with the main rebars in the circumferential direction, as this can ensure a dense mounting point distributed along the cable, which provides a stronger anchorage of the fiber to withstand the high impacts in shotcrete spraying or vibration in concreting. In some cases, the fiber optic cable may be locally routed to span the bars in the longitudinal direction (such as the stirrup bars), as illustrated in Fig. 18d. However, it should be noted that this may not provide sufficient anchorage if the interval distance between two fixing points is large, and the cable may easily displace when subjected to the large external impacts in concreting.

In addition, the fiber optic cable can be continuously bonded on the curved intrados surface of tunnel linings for distributed strain sensing, such as in Gue et al. (2015), Sui et al. (2021) and Gómez et al. (2020). In the study by Gue et al. (2015) the fiber was not prestrained at installation, but the studies by Sui et al. (2021) and Gómez et al. (2020) demonstrate it is practicable to glue the fiber on a curved surface while imposing a small strain (around 0.1%), by a temporary fixing method using tapes and subsequently adding engineering adhesives (like epoxy glue). It must be kept in mind that before gluing fibers on such surfaces, a thorough surface cleaning and preparation is normally necessary for reliable bonding.

Despite the fact that the temperature in underground structures tends to be more stable than that on the surface, temperature effects correction should still be considered, particularly for long-term monitoring. The most common method involves laying an additional temperature-sensing cable parallel to the strain-sensing cable. To retain the temperature fiber at a “strain-free” status, optimally a loose-buffered cable is preferred, with a very stiff jacket or strong tube that will not be significantly compressed when subjected to external forces, such as the cable type utilized in studies by Seo et al. (2017) and Monsberger et al. (2022).

(2) For extensometer use

When the fiber optic cable is installed by point fixing for extensometer use as in Fig. 19a, the essential issue in field instrumentation is a proper fixing method that is capable of imposing the designated prestrain on the gauge lengths and is highly practical for use in field conditions. Note that spot-gluing the fiber directly to the structure surface is mostly not reliably achievable on site, and additional fixing parts are required.

When instrumenting the transverse cross-section of tunnels with optical fiber by point fixing, the “hook and pulley method” proves effective in Mohamad et al. (2012), Gue et al. (2015), and Acikgoz et al. (2017). In this case, hooks are plugged into the holes drilled at specific locations on the tunnel lining, after which a pulley is attached to the hook and the fiber optic cable is prestrained and fixed to the pulley by glue (see Fig. 19c). The “hook and pulley method” is preferable to the “hook method” used in Mohamad et al. (2010) depicted in Fig. 19b, as the pulley can mitigate the sharp curvature on the fiber when it passes through a single hook, which can result in further signal loss associated with small-radius fiber bending. The diameter of the pulley required will be determined by the type of fiber optic cable deployed.

The “hook and pulley method” has been validated as a very convenient and effective way for fiber instrumentation on transverse tunnel cross-sections. However, this method is more applicable when the fiber strain is not high, for instance below 0.3% in

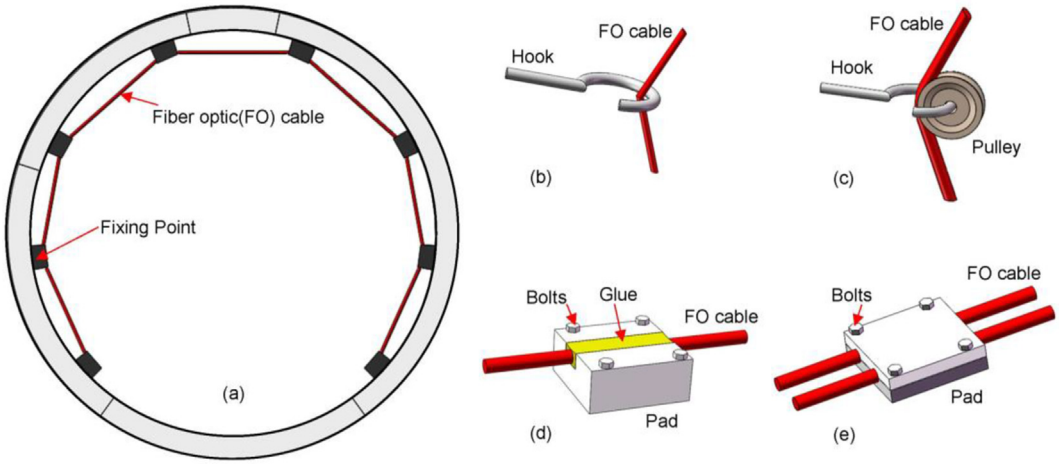

Fig. 19. Fiber optic cable point-fixed to (a) tunnel lining surface with (b) hook method and (c) hook-pulley method; (d) fiber-pad integration with glue and (e) physical clamps.

the studies of Mohamad et al. (2012), Gue et al. (2015), and Acikgoz et al. (2017). Notably, the fiber anchorage by glue at the pulley may be inadequate if the gauge length is strained to a high strain (i.e. above 0.5%), and debonding may occur at the gluing points that further causes an interference of the strain readings between two adjoining fiber sections.

An alternative fiber fixing method is proposed and implemented by Zhu et al., (2022), where a special fixture part is designed and fabricated. This fixture set is composed of a male clamp and a female clamp made of galvanized stainless steel. Four holes are made on the female clamp, with two holes for anchorage on the concrete surface using outer expansion screws, and the other two holes for integrating the male clamp by screws, as shown in Fig. 19e. A thin layer of epoxy resin is used to bind the fiber optic cable to the small slots cut on the clamps to further guarantee the fixing effect and avoid stress localization around clamps.

In the study by Zhang and Broere (2023a), two fiber optic extensometers are combined at an angle to form a joint sensor block for two-direction displacement sensing in an immersed tunnel. For ease of installation, the fiber optic cable is pre-bonded to the narrow slots cut on the fixing pads at the designated locations along the fiber axis, as similar in Fig. 19d. Three fixing pads plus the two interval gauge lengths comprise a sensor block, and in the subsequent field installation, the pads are affixed to the (tiled) tunnel wall surface precisely using adhesive while imposing a prestrain on the fiber, see Fig. 13. Note that in case of a rough bonding surface on the tunnel wall, bolts through the pads can be used as an alternative to the adhesive, as demonstrated in Fig. 19d.

When the fiber optic cable is installed as an extensometer on the structure's surface, a common (loose or tight-buffered) cable from the telecommunication industry can meet the requirement for temperature measurement, as long as it is maintained at zero strain and aligned along with the gauge lengths. Although the sensing fiber optic cable can also be easily extended for temperature sensing, it is often not cost-effective (especially for long-distance sensing) since a dedicated strain sensing fiber can be more expensive than the ordinary communication cable. For some field monitoring applications, such as in Zhang and Broere (2023b), a loose fiber section directly adjoining the strained fiber length can function as a temperature compensation sensor, if the environmental temperature gradient around the sensor is estimated as minor, and this can eliminate the trouble of installing a dedicated temperature sensing fiber.

(3) Instrumentation quality check and protection of fibers/cables

There are several criteria to check the optical fiber instrumentation quality. Firstly, a fast way to check the existence of potential breakage points along the fiber is through a special laser pen, that is readily available commercially. Such a laser pen emits light into the fiber through one end, and at a fiber breakage point the light transmission will stop through the fiber axis; hence no light comes out on the other end. Although this can serve as a quick check that a fiber has been properly installed, it does not necessarily indicate the exact location of any breakages.

The most important aspect when assessing the fiber installation quality is the amount of signal (power) loss. The power loss in the DFOS system can occur through three dominant sources: intrinsic attenuation of the fiber optic cable, loss through connections (including fusing splices and mechanical connectors), and fiber bending. Each interrogator system has its specified minimum signal power for reading, which implies that an excessively high-power loss (exceeding the threshold value) along the cable will fail the measurement. Most interrogators can automatically measure the signal loss (described in dB power loss) along the whole fiber length before starting data acquisition.

Impurities in the fiber core/cladding layers always create an intrinsic attenuation along the fiber optic cable length itself (usually specified by the fiber manufacturer, for instance as an attenuation of 0.5 dB/km), and thus a longer cable suffers a larger power loss. Imperfections in the connections between fiber sections or to the interrogator will induce power loss as well (often around 0.1 dB each), and here usually a fusing splice has a better performance than a mechanical connector and is highly recommended within practical constraints (Gue et al., 2015). These numbers can help users roughly estimate the total intrinsic and connection-related power loss before field installation. Sharp bends in the fiber with a bending radius below the stipulated minimum value (typically specified in the fiber product data sheet), if they occur in a field installation, usually cause a significant power loss that is higher than the intrinsic and connection-related loss, and thus should be avoided by careful handling in the fiber installation.

An interrogator usually can only measure the total signal loss but cannot further distinguish and locate the problematic points along the fiber axis. A more convenient and economical device for signal loss checking that also allows locating problematic locations is the Optic Time Domain Reflectometry (OTDR) interrogator based on Rayleigh scattering. A general OTDR can effectively locate the potential problematic points (connection, breakage, bending points, etc.) and their resulting signal losses along the whole fiber length (Anritsu, 2023), which is quite helpful for the field repair of an installed sensor fiber.

Last but not least, protection of the optical fiber/cable in field conditions is vital for any monitoring work. Many measures can protect the sensing cable part and the connection cables. For example, in the field monitoring by Gómez et al. (2020), the continuously glued optical fiber on the concrete surface was further covered by aluminum tapes externally, as shown in Fig. 20a. In the monitoring study by Zhang and Broere (2023a), the strained fiber lengths installed on the tunnel sidewall are entirely covered by specially designed cover boards made of thin steel plates. These cover boards can not only protect the tensioned fiber from external impacts but also mitigate the airflow-induced vibration on the strained fiber by passing traffic. Besides, the connection fiber sections (loose sections) were also embedded into a PVC duct fixed on top of the road barrier, see Fig. 20b and c. Such protection measures can help reduce the external impacts on the DFOS monitoring network and help sustain the lifetime of the DFOS system.

5. Conclusions

Distributed fiber optic sensor (DFOS) systems can overcome some of the limitations of the current monitoring techniques for underground infrastructure, especially as they allow for continuous distributed sensing instead of taking only localized measurements.

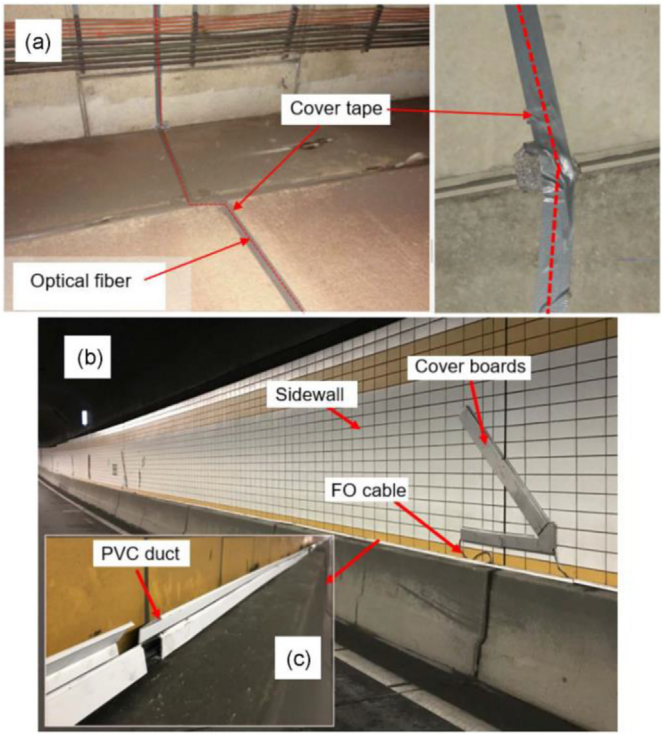

Fig. 20. Optical fiber protection in field conditions: (a) covering by tapes (Gómez et al., 2020); (b) covering by boards, and (c) burial in PVC ducts.

This study presents a comprehensive overview of the emerging use of DFOS for deformation monitoring of tunnel structures, looking at applications for bored tunnels, NATM tunnels, as well as immersed and cut-cover tunnels. The main conclusions are summarized as follows:

(1) DFOS has been successfully utilized to instrument various types of tunnel structures, enabling both distributed strain measurements along the fiber and point displacement measurements at specific locations. These monitoring results can be used to determine the tunnel's transverse deformation behavior as well as longitudinal flexural behavior and establish the amount of localized displacement at the joints.

(2) The performance of a DFOS system in tunnel monitoring typically depends on four aspects: the selection of the working principle (interrogator system), the selection of the optimal sensing fiber, the design of an effective sensor layout, and the establishment of robust field sensor instrumentation. DFOS based on OFDR typically has a high spatial resolution, but a significantly reduced sensing distance, making it ideal for precise distributed strain sensing in small to medium-scale experiments, or field monitoring of local tunnel sections. In contrast, DFOS based on Brillouin scattering has a lower spatial resolution, but allows for a significantly greater sensing distance, making it optimal for field applications in long tunnel infrastructure.

(3) An effective sensor layout should consider the expected range of observed strain in the fiber, establish an explicit transfer relation from fiber strain to the target observable (displacement, flexural deflection, etc.) that corrects for temperature influences, and takes the ease of field installation as well as the protection of the fiber during tunnel operation into account.

(4) For newly built tunnels the fiber can be embedded into the tunnel lining. In NATM tunnels this can be achieved by securing the fiber to the rebar prior to concreting on site, whereas for bored and immersed tunnels either special ducts have to be prepared in the segments, allowing for later fiber installation, or the fiber has to be embedded in individual segments during segment production, and in that case, the individual fiber sections have to be spliced together on site later. For existing tunnels, the sensor layout is typically limited to a cable continuously bonded (for distributed strain sensing) or fixed at discrete points (for extensometer use) along the inner surface to monitor the transverse oblique and vertical ovalization deformation modes. When fixing the fiber at discrete points, care should be taken to avoid sharp bends in the fiber leading to signal loss, caused for example by spot gluing the fiber onto steel hooks only.

(5) When monitoring the tunnel's transverse behavior, the combined axial-flexural deformation mode can be obtained from the distributed strain, in which case a fiber layout with two parallel fiber optic cables embedded inside the tunnel lining is preferable. For the longitudinal behavior, the flexural deformation of bored tunnels can be observed by monitoring the circumferential joint deformations using fiber optic extensometers installed across the joint gaps. In general, local deformations at tunnel joints can be effectively measured by single or combined fiber optic extensometers placed across the joint gap, and such layouts have been demonstrated to work successfully in both bored and immersed tunnels. Finally, in NATM tunnels the settlement of surrounding soil near the tunnel crown can be effectively monitored by fiber optic cables embedded longitudinally into the lining or mounted at discrete spots on the lining surface.

In summary, DFOS has been successfully implemented in a number of tunnel monitoring projects, for both bored, immersed, and conventional tunnels. It has demonstrated great potential as it allows for both distributed strain and displacement monitoring at higher densities of cost-effective monitoring points than conventional techniques.

Declaration of competing interest

The authors declare that they have no known competing financial interests or personal relationships that could have appeared to influence the work reported in this paper.

Acknowledgments

We acknowledge the funding support from Rijkswaterstaat, the Netherlands, and European Union's Horizon 2020 Research and Innovation Programme (Project SAFE-10-T under Grant No. 723254), China Scholarship Council, and National Natural Science Foundation of China (Grant No. 42225702).

References

Acikgoz, S., Pelecanos, L., Giardina, G., Aitken, J., Soga, K., 2017. Distributed sensing of a masonry vault during nearby piling. Struct. Control Health Monit. 24, e1872.
Anritsu, 2023. OTDR device information. https://www.anritsu.com/en-us/test-measurement/products/mt1000a. (Accessed 30 September 2023).
Broere, W., 2016. Urban underground space: solving the problems of today's cities. Tunn. Undergr. Space Technol. 55, 245–248.
Buchmayer, F., Monsberger, C.M., Lienhart, W., 2021. Advantages of tunnel monitoring using distributed fibre optic sensing. J. Appl. Geodesy 15 (1), 1–12.
Ceyear, 2023. Product specification of AV6419 type BOTDR. https://ceyear.com/optical_link_test-9. (Accessed 1 September 2023).
Chapman, D.N., Metje, N., Stark, A., 2017. Introduction to Tunnel Construction, second ed. CRC Press, Taylor & Francis Group, Boca Raton, FL, USA.
Chai, J., Wang, Z., Lei, W., Du, W., Zhang, D., 2021. Research on the key technology of distributed fiber monitoring in tunnel bottom drum. IOP conference series. Earth and Environ. Sci. 861 (4), 42052.
Cheung, L.L.K., Soga, K., Bennett, P.J., Kobayashi, Y., Amatya, B., Wright, P., 2010. Optical fibre strain measurement for tunnel lining monitoring. Proc. Inst. Civ. Eng. Geotech. Eng. 163 (3), 119–130.
Corning, 2021. Corning optic fiber product information. https://www.corning.com/media/worldwide/coc/documents/Fiber/PI-1463-AEN.pdf. (Accessed 1 December 2021).
Cui, J., Broere, W., Lin, D., 2021a. Underground space utilisation for urban renewal. Tunn. Undergr. Space Technol. 108, 103726.
Cui, Y., Li, Z., Wei, G., Chen, J., Zhou, L., 2021b. Pre-protection effect of underground comprehensive pipe gallery over proposed tunnel. J. Zhejiang Univ. (Eng. Sci.) 55 (2), 330–337.
De Battista, N., Elshafie, M.Z.E.B., Soga, K., Williamson, M., Hazelden, G., Hsu, Y.S., 2015. Strain monitoring using embedded distributed fibre optic sensors in a sprayed concrete tunnel lining during the excavation of cross-passages. In: Proceedings of the 7th International Conference on Structural Health Monitoring of Intelligent Infrastructure, pp. 1–3. Torino, Italy.
Di Murro, V., Pelecanos, L., Soga, K., Kechavarzi, C., Morton, R.F., Scibile, L., 2019. Long-term Deformation Monitoring of CERN concrete-lined tunnels using distributed fibre-optic sensing. Geotech. Eng. J. SEAGS & AGSSEA 50 (2), 1–7.
Fibristerre, 2022. Information of BOFDA interrogator. https://www.fibristerre.de/files/fibrisTerre_flyer.pdf. (Accessed 20 June 2022).
Gao, Y., Zhu, H., Qiao, L., Liu, X., Wei, C., Zhang, W., 2023. Feasibility study on sinkhole monitoring with fiber optic strain sensing nerves. J. Rock Mech. Geotech. Eng. 15 (11), 3059–3070.
Gavin, K.G., Broere, W., Kovačević, M.S., de Haas, K., 2019. Investigation of the remaining life of an immersed tube tunnel in The Netherlands. In: Proceedings of the WTC 2019 ITA-AITES World Tunnel Congress (WTC 2019), p. 4831. Naples, Italy.
Gong, H., Kizil, M.S., Chen, Z., Amanzadeh, M., Yang, B., Aminossadati, S.M., 2019. Advances in fibre optic based geotechnical monitoring systems for underground excavations. Int. J. Min. Sci. Technol. 29 (2), 229–238.
Grunicke, U.H., Lienhart, W., Vorwagner, A., 2021. Long-term monitoring of visually not inspectable tunnel linings using fibre optic sensing. Geomech. Tunn. 14 (1), 19–32.
Gue, C.Y., Wilcock, M., Alhaddad, M.M., Elshafie, M.Z.E.B., Soga, K., Mair, R.J., 2015. The monitoring of an existing cast iron tunnel with distributed fibre optic sensing (DFOS). J. Civ. Struct. Health Monit. 5 (5), 573–586.
Gómez, J., Casas, J.R., Villalba, S., 2020. Structural health monitoring with distributed optical fiber sensors of tunnel lining affected by nearby construction activity. Autom. ConStruct. 117, 103261.
Guo, W., Feng, K., Lu, X., Qi, M., He, C., Xiao, M., Zuo, L., 2023. Experimental investigation on the damage evolution and failure mechanism of segmental joints based on DOFS and AE. Eng. Fail. Anal. 152, 107471.
Hartog, A., 2017. An Introduction to Distributed Optical Fiber Sensors. CRC Press, Taylor & Francis Group, Boca Raton, FL, USA.
Hong, C., Zhang, Y., Li, G., Zhang, M., Liu, Z., 2017. Recent progress of using Brillouin distributed fiber optic sensors for geotechnical health monitoring. Sensor Actuator Phys. 258, 131–145.
Hong, C., Zhou, Z., Chen, W., Fu, Y., Shen, X., 2022. Segment monitoring of shield tunnel crossing fracture zone based on optical frequency domain reflectometry. Tunn. Constr. 42 (10), 1729 (in Chinese).
Hou, G., Xi, B., Xie, B., Wei, G., Li, Z., 2017. Theoretical and experimental study of the relationship between optical fiber strain and settlement of roof based on BOTDR technology. Rock Soil Mech. 38 (5), 1298–1304.
Hou, G., Han, Y., Xie, B., Wei, G., Li, Z., Xiao, H., Zhou, T., 2019. Pretension strain loss of fixed-point optical fiber in tunnel structural health monitoring. Rock Soil Mech. 40 (10), 4120–4127.
Hou, G., Li, Z., Hu, T., Zhou, T., Xiao, H., 2020. Study on boundary effect of embedded optical fiber sensor in tunnel structure. Rock Soil Mech. 41 (8), 2839–2850.
Hou, G., Li, Z., Hu, Z., Feng, D., Zhou, H., Cheng, C., 2021. Method for tunnel cross-section deformation monitoring based on distributed fiber optic sensing and neural network. Opt. Fiber Technol. 67, 102704.
Housner, G., Bergman, L.A., Caughey, T.K., Chassiakos, A.G., Claus, R.O., Masri, S.F., Skelton, R.E., Soong, T.T., Spencer, B.F., Yao, J.T.P., 1997. Structural control: past, present, and future. J. Eng. Mech. 123 (9), 897–971.
Hruby, D., Cubik, J., Jaros, J., Kepak, S., Zabka, S., Mec, P., Vasinek, V., 2019. Distributed fibre-optic technology for security monitoring of a structural load of road and motorway tunnels. In: Proceedings of the 4th International Conference on Civil, Structural and Transportation Engineering. ICCSTE'19), Ottawa, Canada.
Huang, J., Yan, Z., Li, D., Tang, X., Yao, X., 2021. In-situ experimental study on deformation behaviors of lining structure for shield tunnels under high internal pressure. J. Hydroelectr. Eng. 40 (3), 165–172 (in Chinese).
Imai, M., Mizuno, S., 2020. Aqueduct tunnel convergence measurement using a distributed optical fiber sensor. In: Optical Fiber Sensors Conference 2020 Special Edition. Optica Publishing Group paper T3.22.
Jiao, T., Zhou, Z., 2021. An optical-electrical co-sensing tape for cross-sectional deformation monitoring of shield tunnels. Tunn. Undergr. Space Technol. 117, 104148.
Karakuş, M., Fowell, R.J., 2004. An insight into the new Austrian tunnelling method (NATM). In: Proceedings of ROCKMEC'2004-VIIth Regional Rock Mechanics Symposium 2004. Sivas, Turkey.
Kechavarzi, C., Soga, K., De Battista, N., Pelecanos, L., Elshafie, M.Z.E.B., Mair, R.J., 2015. Distributed Fibre Optic Strain Sensing for Monitoring Civil Infrastructure. ICE publishing, London, UK.
Kreger, S.T., Gifford, D.K., Froggatt, M.E., Soller, B.J., Wolfe, M.S., 2006. High resolution distributed strain or temperature measurements in single-and multi-mode fiber using swept-wavelength interferometry. In: Optical Fiber Sensors. Optica Publishing Group, Washington, DC, USA, p. ThE42.
Leung, C.K., Wan, K.T., Inaudi, D., Bao, X., Habel, W., Zhou, Z., Imai, M., 2015. Optical fiber sensors for civil engineering applications. Mater. Struct. 48 (4), 871–906.
Li, C., Sun, Y., Zhao, Y., Liu, H., Gao, L., Zhang, Z., Qiu, H., 2006. Monitoring pressure and thermal strain in the second lining of a tunnel with a Brillouin OTDR. Smart Mater. Struct. 15 (5), 107–110.
Li, Y.H., Xu, S.D., Liu, J.P., 2015. A new convergence monitoring system for tunnel or drift based on draw-wire displacement sensors. Tunn. Undergr. Space Technol. 49, 92–97.
Li, Z., Hou, G., Hu, T., Zhou, T., Xiao, H., 2020. A study on the application of the distributed optical fiber sensing monitoring technology in the process of dismantling temporary tunnel shoring. Arabian J. Geosci. 13 (19), 1–11.
Li, H., Xu, Q., Liu, Y., 2021. Method for diagnosing the uneven settlement of a rail transit tunnel based on the spatial correlation of high-density strain measurement points. Sustainability 13 (16), 9245.
Li, M., Shao, G., Han, G., Yu, B., Yang, T., Hu, Z., 2022. Design and layout path of optical fiber monitoring system for shield tunnel. J. Wuhan Univ. Technol. (Inf. Manag. Eng.) 44 (6), 78–83 (in Chinese).
Li, H., Zhu, H., Tan, D., Shi, B., Yin, J., 2023. Detecting pipeline leakage using active distributed temperature Sensing: theoretical modeling and experimental verification. Tunn. Undergr. Space Technol. 135, 105065.
Lienhart, W., Moser, F., Schuller, H., Schachinger, T., 2014. Reinforced earth structures at Semmering base tunnel—construction and monitoring using fiber optic strain measurements. In: Proceedings of the 10th International Conference on Geosynthetics (10ICG), Deutsche Gesellschaft Fuer Geotechnik (DGGT). Essen, Germany.
Liu, Q., Wang, J., Xiao, L., Li, J., Liu, B., Zhang, X., 2017. Application of OFDR-based sensing technology in geo-mechanical model test on tunnel excavation using

cross rock pillar method. Chin. J. Rock Mech. Eng. 36 (5), 1063–1075 (in Chinese).
Liu, J., Omar, H., Sian, K.D., Liu, J., 2018. Repairing a shield tunnel damaged by secondary grouting. Tunn. Undergr. Space Technol. 80, 313–321.
Liu, T., Chen, G., Tang, X., Zhang, W., Huang, H., Yao, G., 2020. The bearing mechanism of superimposed linings structure under high inner hydraulic pressure: a prototype experimental study. J. Hydraul. Eng. 51 (3), 295–304 (in Chinese).
López-Higuera, J.M., 1998. Optical Sensors. Editorial Universidad de Cantabria, Cantabria, Spain.
López-Higuera, J.M., Cobo, L.R., Incera, A.Q., Cobo, A., 2011. Fiber optic sensors in structural health monitoring. J. Lightwave Technol. 29 (4), 587–608.
Luna, 2022. ODiSI 6000 series optical distributed sensor interrogator. https://lunainc.com/product/odisi-6000-series. (Accessed 1 December 2022).
Lunniss, R., Baber, J., 2013. Immersed Tunnels. CRC Press, Taylor & Francis Group, Boca Raton, FL, USA.
Lu, X., Feng, K., Qi, M., Guo, W., 2023. Experimental study on deformation behavior of shield tunnel subjected to riverbed scour based on DOFS. KSCE J. Civ. Eng. 27 (4), 1800–1819.
Ma, J., Pei, H., Zhu, H., Shi, B., Yin, J., 2022. A review of previous studies on the applications of fiber optic sensing technologies in geotechnical monitoring. Rock Mech. Bull. (Arch. Am. Art) 2 (1), 100021.
Mao, J., He, Y., Jin, W., 2011. Life-cycle stress monitoring method for tunnel secondary lining based on distributed optical fiber sensor. China J. Highway Transport 24 (2), 77–82 (in Chinese).
Mega-sense, 2022. OSI-S high-precision distributed optical fiber sensing monitoring system. https://www.mega-sense.com/OSI-S.html. (Accessed 1 December 2022).
Minardo, A., Catalano, E., Coscetta, A., Zeni, G., Di Maio, C., Vassallo, R., Zeni, L., 2021. Long-term monitoring of a tunnel in a landslide prone area by brillouin-based distributed optical fiber sensors. Sensors 21 (21), 7032.
Moffat, R., Sotomayor, J., Beltrán, J.F., 2015. Estimating tunnel wall displacements using a simple sensor based on a Brillouin optical time domain reflectometer apparatus. Int. J. Rock Mech. Min. Sci. 75, 233–243.
Mohamad, H., Bennett, P.J., Soga, K., Mair, R.J., Bowers, K., 2010. Behaviour of an old masonry tunnel due to tunnelling-induced ground settlement. Geotechnique 60 (12), 927–938.
Mohamad, H., Soga, K., Bennett, P.J., Mair, R.J., Lim, C.S., 2012. Monitoring twin tunnel interaction using distributed optical fiber strain measurements. J. Geotech. Geoenviron. Eng. 138 (8), 957–967.
Monsberger, C.M., Lienhart, W., Moritz, B., 2018. In-situ assessment of strain behaviour inside tunnel linings using distributed fibre optic sensors. Geomech. Tunn. 11 (6), 701–709.
Monsberger, C.M., Bauer, P., Buchmayer, F., Lienhart, W., 2022. Large-scale distributed fiber optic sensing network for short and long-term integrity monitoring of tunnel linings. J. Civ. Struct. Health Monit. 12 (6), 1317–1327.
Monsberger, C.M., Lienhart, W., 2021. Distributed fiber optic shape sensing along shotcrete tunnel linings: methodology, field applications, and monitoring results. J. Civ. Struct. Health Monit. 11 (2), 337–350.
Motil, A., Bergman, A., Tur, M., 2016. State of the art of brillouin fiber-optic distributed sensing. Opt Laser. Technol. 78, 81–103.
Mo, W., Yang, Y., Lin, Y., Lu, M., 2022. Measurement and calculation method for shield tunnel segment dislocation deformation based on OFDR technology. Modern tunn. Technol. 59 (5), 179–187.
Nanzee Sensing, 2022. Optical fiber cable products information. http://www.nzsensing.com/cpzx/info_3.aspx?itemid=475. (Accessed 1 June 2022).
Naruse, H., Uehara, H., Deguchi, T., Fujihashi, K., Onishi, M., Espinoza, R., Pinto, M., 2007. Application of a distributed fibre optic strain sensing system to monitoring changes in the state of an underground mine. Meas. Sci. Technol. 18 (10), 3202–3210.
Neubrex, 2022. Product information BOTDA measurement unit. https://www.neubrex.com/htm/products/pro-nbx-lineup.htm. (Accessed 1 June 2023).
OZ Optics, 2022. Product brochure Foresight™ series interrogator. https://www.ozoptics.com/products/fiber_optic_distributed.html. (Accessed 30 July 2022).
Radončić, N., Kern, M., Weissnar, M., Moritz, B., 2015. Strain gauges in pre-cast concrete segments: working principle, evaluation and interpretation. Geomech. Tunn. 8 (3), 265–272.
Roca-Pardinas, J., Argueelles-Fraga, R., Lopez, F.D.A., Ordonez, C., 2014. Analysis of the influence of range and angle of incidence of terrestrial laser scanning measurements on tunnel inspection. Tunn. Undergr. Space Technol. 43, 133–139.
Schenato, L., Bossi, G., Marcato, G., Pasuto, A., 2016. Cumulative monitoring of strain in concrete structures with polymer optical fibers. Rendiconti Online della Società Geologica Italiana 39, 19–22.
Seo, H., Wilcock, M.J., Soga, K., Elshafie, M., Mair, R.J., 2017. Distributed fibre optic monitoring of the time-dependent behaviour of tunnel segmental linings in London clay. In: Proceedings of the 2017 World Congress on Advances in Structure Engineering and Mechanics. Seoul, Korea.
Shen, S., Wu, Z., Yang, C., Hong, W., Tang, Y., Wu, G., 2013. Convergence deformation monitoring of shield tunnels based on distributed optical fiber strain sensing technique. China Civ. Eng. J. 46 (9), 104–116 (In Chinese).
Shi, B., Xu, X.J., Wang, D., Wang, T., Cui, H.L., 2005. Study on BOTDR-based distributed optical fiber strain measurement for tunnel health diagnosis. Chin. J. Rock Mech. Eng. 24 (15), 2622–2627 (In Chinese).
Smartec, 2022. DiTeSt dual reading unit information. https://smartec.ch/en/product/ditest-reading-unit-2/. (Accessed 30 December 2022).
Soga, K., 2014. Understanding the real performance of geotechnical structures using an innovative fibre optic distributed strain measurement technology. Rivista Italiana di Geotechnica 4, 7–48.
Solifos AG, 2023. BRUsens DSS V3 and V9 strain cable information. https://solifos.com/en/sensing/structural-health-monitoring. (Accessed 30 September 2023).
Sui, Y., Cheng, X., Wei, J., 2021. Distributed fibre optic monitoring of damaged lining in double-arch tunnel and analysis of its deformation mode. Tunn. Undergr. Space Technol. 110, 103812.
Sui, Y., Cheng, X., Li, G., Pu, L., Li, C., Liao, P., 2022. Inversion analysis of deformation and force of shield tunnel segments based on distributed optical-fibre monitoring. Eng. Mech. 39 (S), 158–163 (In Chinese).
Tan, X., Fan, L., Bao, Y., 2021. Detection, visualization, quantification, and warning of pipe corrosion using distributed fiber optic sensors. Autom. ConStruct. 132, 103953.
Thomas, A., 2019. Sprayed Concrete Lined Tunnels, second ed. CRC Press, Taylor & Francis Group, Boca Raton, FL, USA.
Wagner, L., Kluckner, A., Monsberger, C.M., Wolf, P., Prall, K., Schubert, W., Lienhart, W., 2020. Direct and distributed strain measurements inside a shotcrete lining: concept and realisation. Rock Mech. Rock Eng. 53 (2), 641–652.
Wang, D., Zhu, H., Huang, J., Yan, Z., Zheng, X., Shi, B., 2023a. Fiber optic sensing and performance evaluation of a water conveyance tunnel with composite linings under super-high internal pressures. J. Rock Mech. Geotech. Eng. 15 (8), 1997–2012.
Wang, F., Huang, H., Zhang, D., Zhang, W., Xu, R., 2013. Deformation sensing method of shield tunnel based on optical fiber sensing technology of BOTDA. Chin. J. Rock Mech. Eng. 32 (9), 1901–1908 (In Chinese).
Wang, H., Zhang, D., Ren, K., Shi, B., Guo, J., Sun, M., 2023b. The sensing performance of a novel optical cable for tunnel water leakage monitoring based on distributed strain Sensing. IEEE Sensor. J. 23 (19), 22496–22506.
Wang, J., Zhu, H., Tan, D., Li, Z., Li, J., Wei, C., Shi, B., 2023c. Thermal integrity profiling of cast-in-situ piles in sand using fiber-optic distributed temperature sensing. J. Rock Mech. Geotech. Eng. 15 (12), 3244–3255.
Wang, Q., Gu, X., Zhang, Z., Long, Z., Zhao, Y., 2022. On-line leakage detection in buried tap water distribution pipes using distributed temperature sensing. J. Pipeline Syst. Eng. Pract. 13 (2), 04022010.
Wang, S., Zhang, X., Bai, Y., 2020. Comparative study on foundation treatment methods of immersed tunnels in China. Front. Struct. Civ. Eng. 14 (1), 82–93.
Wang, X., Shi, B., Wei, G., Chen, S., Zhu, H., Wang, T., 2018. Monitoring the behavior of segment joints in a shield tunnel using distributed fiber optic sensors. Struct. Control Health Monit. 25 (2), e2056.
Wijaya, H., Rajeev, P., Gad, E., 2021. Distributed optical fibre sensor for infrastructure monitoring: field applications. Opt. Fiber Technol. 64, 102577.
Wuilpart, M., 2011. Rayleigh scattering in optical fibers and applications to distributed measurements. In: Advanced Fiber Optics: Concepts and Technology, Thévanez, Luc. EPFL Press, Lausanne, Switzerland.
Xu, D.S., Zhao, Y.M., Liu, H.B., Zhu, H.H., 2017. Deformation monitoring of metro tunnel with a new ultrasonic-based system. Sensors 17 (8), 1758.
Xu, D., Zhang, X., Chen, W., Jiang, X., Liu, Z., Bai, Y., 2019. Utilisation of the deep underground space in Shanghai. Proc. Inst. Civ. Eng.: Munic. Eng. 172 (4), 218–223.
Xue, X., Xie, Y., Zhou, X., 2019. Study on the life-cycle health monitoring technology of water-rich loess tunnel. Adv. Mater. Sci. Eng. 2019, 1–12.
Yuan, Y., Bai, Y., Liu, J., 2012. Assessment service state of tunnel structure. Tunn. Undergr. Space Technol. 27 (1), 72–85.
Yao, G., 2023. Research on invert monitoring system of expansive rock tunnel based on distributed optical fiber. In: 5th International Conference on Intelligent Control, Measurement and Signal Processing (ICMSP). IEEE, New York, United States, pp. 181–184.
Yang, F., Feng, X., Zhang, J., Zhong, G., Yuan, Y., 2023. Structural damage identification of subseabed shield tunnels based on distributed fiber optic sensors and information fusion. Tunn. Undergr. Space Technol. 139, 105215.
Zhang, C.C., Zhu, H.H., Liu, S.P., Shi, B., Cheng, G., 2020. Quantifying progressive failure of micro-anchored fiber optic cable–sand interface via high-resolution distributed strain sensing. Can. Geotech. J. 57 (6), 871–881.
Zhang, X., Wu, X., Broere, W., 2021. Impact of Subsoil Spatial Variability on Deformations of Immersed Tunnel. Geotechnical Aspects of Underground Construction in Soft Ground. CRC Press, Taylor & Francis Group, Boca Raton, FL, USA, pp. 738–745.
Zhang, J., Yan, Q., Li, W., Su, L., Sun, M., Yao, C., 2022a. Failure analysis of a new-type shield tunnel based on distributed optical fiber sensing technology. Eng. Fail. Anal. 142, 106748.
Zhang, L., Cui, Y., Shi, B., 2022b. Complex deformation monitoring of shield tunnel segment joints using distributed fiber optic sensing technology: experimental verification. IEEE Sensor. J. 22 (4), 3236–3245.
Zhang, X., Broere, W., 2022. Sensing fiber selection for point displacement measuring with distributed optic fiber sensor. Measurement 197, 111275.

Zhang, X., Broere, W., 2023a. Design of a distributed optical fiber sensor system for measuring immersed tunnel joint deformations. Tunn. Undergr. Space Technol. 131, 104770.
Zhang, X., Broere, W., 2023b. Monitoring of tidal variation and temperature change-induced movements of an immersed tunnel using distributed optical fiber sensors (DOFSs). Struct. Control Health Monit. 2023, 2419495.
Zheng, Y., Zhu, Z.W., Xiao, W., Deng, Q.X., 2020. Review of fiber optic sensors in geotechnical health monitoring. Opt. Fiber Technol. 54, 102127.
Zhou, Z., Liu, Y., Li, H., 2023. A method for convergence monitoring considering the flattening effect in a shield tunnel with BOTDA sensors. Measurement 211, 112611.
Zhu, G., Feng, X., Zhou, Y.Y., Li, Z.W., Fu, L.J., Xiong, Y.R., 2020. Physical model experimental study on spalling failure around a tunnel in synthetic marble. Rock Mech. Rock Eng. 53 (2), 909–926.
Zhu, H.H., Wang, D.Y., Shi, B., Wang, X., Wei, G.Q., 2022. Performance monitoring of a curved shield tunnel during adjacent excavations using fiber optic nervous sensing system. Tunn. Undergr. Space Technol. 124, 104483.
Zhu, H.H., Wang, Z.Y., Shi, B., Wong, J.K.W., 2016. Feasibility study of strain-based stability evaluation of locally loaded slopes: insights from physical and numerical modeling. Eng. Geol. 208, 39–50.

Dr. Wout Broere is the associate professor of Underground Space Technology at Delft University of Technology (TU Delft), Netherlands. He obtained his MSc degree in 1996 and PhD degree in 2001, both at TU Delft. After obtaining his PhD, he became an independent geotechnical consultant and has worked as head of courses and support at Plaxis BV while continuing as a part-time researcher at TU Delft. Since 2006, he has held a full-time position at TU Delft. His research interests include trenchless technologies, underground construction in soft soils, the use of underground space, foundation engineering, physical modeling and centrifuge testing, site investigation and laboratory testing. He provided geotechnical expertise for several large tunneling projects in the Netherlands and abroad, including Groene Hart and Liefkenshoek, as well as on foundation engineering aspects for onshore and offshore foundations. Currently, he serves as the Editor-in-Chief of Tunneling and Underground Space Technology and is a Board Member of ISTT International Society for Trenchless Technologies.